TKK Dissertations 214
Espoo 2010

DYE-SENSITIZED SOLAR CELLS ON ALTERNATIVE SUBSTRATES

Doctoral Dissertation

Minna Toivola

Aalto University
School of Science and Technology
Faculty of Information and Natural Sciences
Department of Applied Physics

TKK Dissertations 214
Espoo 2010

DYE-SENSITIZED SOLAR CELLS ON ALTERNATIVE SUBSTRATES

Doctoral Dissertation

Minna Toivola

Doctoral dissertation for the degree of Doctor of Science in Technology to be presented with due permission of the Faculty of Information and Natural Sciences for public examination and debate in Auditorium K216 at the Aalto University School of Science and Technology (Espoo, Finland) on the 16th of April 2010 at 12 noon.

Aalto University
School of Science and Technology
Faculty of Information and Natural Sciences
Department of Applied Physics

Aalto-yliopisto
Teknillinen korkeakoulu
Informaatio- ja luonnontieteiden tiedekunta
Teknillisen fysiikan laitos

Distribution:
Aalto University
School of Science and Technology
Faculty of Information and Natural Sciences
Department of Applied Physics
P.O. Box 14100
FI - 00076 Aalto
FINLAND
URL: http://tfy.tkk.fi/
Tel. +358-9-470 23198
Fax +358-9-470 23195
E-mail: eila.jylkas@tkk.fi

ISBN 978-952-60-3069-2
ISBN 978-952-60-3070-8 (PDF)
ISSN 1795-2239
ISSN 1795-4584 (PDF)
URL: http://lib.tkk.fi/Diss/2010/isbn9789526030708/

TKK-DISS-2734

Aalto-Print
Helsinki 2010

Aalto University

ABSTRACT OF DOCTORAL DISSERTATION	AALTO UNIVERSITY SCHOOL OF SCIENCE AND TECHNOLOGY P.O. BOX 11000, FI-00076 AALTO http://www.aalto.fi

Author Minna Toivola

Name of the dissertation
Dye-sensitized solar cells on alternative substrates

Manuscript submitted 29.10.2009	Manuscript revised 8.2.2010
Date of the defence 16.4.2010	
☐ Monograph	☒ Article dissertation (summary + original articles)

Faculty	Faculty of Information and Natural Sciences
Department	Department of Applied Physics
Field of research	New Energy Technologies
Opponent(s)	Prof. Michael Grätzel
Supervisor	Prof. Peter Lund
Instructor	Prof. Peter Lund

Abstract

Dye-sensitized solar cells (DSC) could become a potential alternative for the traditional silicon and thin film panels in the near future, due to the DSC's for the most part cheap materials and simple manufacturing methods. One of the challenges of this technology is, however, the heavy, expensive and inflexible glass substrate typically used in the cells. To address this problem, this thesis concentrates on transfer of the DSC technology from glass substrates to light weight, cost-efficient, and flexible plastic foils and metal sheets. Flexible solar cell would be well suited for industrial-scale mass production, for example with roll-to-roll methods and when integrated on building materials it could work as a functional coating, enabling electricity-producing roofing or façade structures.

In the course of this thesis, DSCs were prepared on ITO-PET and ITO-PEN plastics, stainless steel (StS), and optical fibers. Due to the low temperature tolerance of the plastics, development and characterization of room temperature processable counter electrode materials suitable for these substrates was a part of this work. Powder suspension based on carbon nanoparticles proved to be an easily depositable, cost-efficient material with catalytic activity as high as that of platinum. With metal materials, the main problem is the corrosive, iodine-based electrolyte conventionally used in the DSC. This is why, in the beginning of this work, the corrosion resistance of some widely used building materials such as zinc-coated carbon steels, copper, and StS was studied with soaking tests in the electrolyte. StS passed the soaking tests and was chosen for further research. StS has also other benefits such as good electrical conductivity and mechanical sturdiness. Substrate-mediated leakage current is also smaller from StS than from glass substrates. With a DSC configuration where the StS sheet worked as the photoelectrode substrate efficiencies comparable to all-glass cells, near 5 %, were obtained so this configuration was chosen also for the cell size upscaling tests. The largest StS photoelectrode cells prepared in the course of this thesis were 6 cm x 6 cm and their efficiencies over 3 % at their best. This is already a promising value considering the ohmic losses bound to happen at the counter electrode, due to the sheet resistance of the counter electrode substrate. To minimize these losses, additional current collector structures were integrated on the counter electrode substrate with inkjet-printing with silver nanoparticle ink. 50 % reduction in the total ohmic losses of the cell was achieved with the current collector structures and 80 % with replacing the photoelectrode glass substrate with the StS sheet.

StS-based DSC would seem like a feasible concept even for industrial-scale mass production but special emphasis should be put, in the future research, on the long term stability of the cells and its improvement. Room for improvement still exists in efficiencies also – a research challenge in which for example some recently developed carbon nanomaterials might provide progress.

Keywords dye solar cell, plastic substrate, metal substrate, nanomaterials

ISBN (printed) 978-952-60-3069-2	ISSN (printed) 1795-2239
ISBN (pdf) 978-952-60-3070-8	ISSN (pdf) 1795-4584
Language English	Number of pages 64 p. + app. 91 p.

Publisher Aalto University School of Science and Technology

Print distribution Department of Applied Physics

☒ The dissertation can be read at http://lib.tkk.fi/Diss/2010/isbn9789526030708/

Aalto-yliopisto

VÄITÖSKIRJAN TIIVISTELMÄ	AALTO-YLIOPISTO TEKNILLINEN KORKEAKOULU PL 11000, 00076 AALTO http://www.aalto.fi

Tekijä Minna Toivola

Väitöskirjan nimi
Väriaineherkistetyt aurinkokennot vaihtoehtoisilla alustoilla

Käsikirjoituksen päivämäärä 29.10.2009	Korjatun käsikirjoituksen päivämäärä 8.2.2010

Väitöstilaisuuden ajankohta 16.4.2010

☐ Monografia	☒ Yhdistelmäväitöskirja (yhteenveto + erillisartikkelit)

Tiedekunta	Informaatio- ja luonnontieteiden tiedekunta
Laitos	Teknillinen fysiikka
Tutkimusala	Energiatieteet
Vastaväittäjä(t)	Prof. Michael Grätzel
Työn valvoja	Prof. Peter Lund
Työn ohjaaja	Prof. Peter Lund

Tiivistelmä

Väriaineherkistetyn nanoaurinkokennon suurimmaksi osaksi edullisista valmistusmateriaaleista ja kennon yksinkertaisesta valmistettavuudesta johtuen tästä teknologiasta ennustetaan lähitulevaisuudessa potentiaalista vaihtoehtoa nyt yleisesti käytössä oleville pii- ja ohutkalvopaneeleille. Eräs väriaineaurinkokennon ongelmista on kuitenkin raskas, kallis ja joustamaton lasisubstraatti, jolle kennot on tyypillisesti valmistettu. Tässä työssä onkin tutkittu kuinka kennoteknologia saataisiin siirrettyä lasisubstraateilta kevyille, taipuisille ja edullisille muovikalvoille ja metallilevyille. Joustava kenno soveltuisi hyvin myös teolliseen massatuotantoon, valmistettavaksi kelalta-kelalle –menetelmillä. Rakennusmateriaaleihin integroituna se voisi taas toimia funktionaalisena pinnoitteena, mahdollistaen esim. sähköä tuottavat katto- tai fasadirakenteet.

Tämän työn aikana valmistettiin väriaineaurinkokennoja ITO-PET ja ITO-PEN –muoveille, ruostumattomalle teräkselle (RST) ja optisille valokuiduille. Koska muovisubstraatit eivät kestä korkeita lämpötiloja, eräs työn osa-alue oli muoveille soveltuvien, huoneen lämpötilassa prosessoitavien vastaelektrodimateriaalien kehittäminen ja karakterisointi. Hiilinanopartikkelipohjainen pulverisuspensio osoittautui helposti depositoitavaksi ja edulliseksi materiaaliksi, jonka katalyyttinen aktiivisuus oli parhaimmillaan platinan luokkaa. Metallimateriaalien käyttöä väriaineaurinkokennossa rajoittaa kennon jodipohjainen elektrolyytti, joka korrondoi monia metalleja. Työn aluksi selvitettiinkin yleisesti käytettyjen rakennusmetallien sinkityn hiiliteräksen, kuparin ja ruostumattoman teräksen korroosiokestävyys liuotuskokein elektrolyytissä. RST läpäisi liuotuskokeet ja valittiin näin ollen jatkotutkimuksiin. RST:llä on myös muita etuja, mm. hyvä sähkönjohtavuus, mekaaninen kestävyys ja pienempi vuotovirta substraatista elektrolyyttiin. RST-valoelektrodipohjaisella kennokonfiguraatiolla saavutettiinkin lasikennoon verrattava hyötysuhde, lähes 5 %, joten tämä konfiguraatio valittiin myös kennon koon kasvatuskokeisiin. Suurimmat työn aikana valmistetut RST-valoelektrodikennot olivat kooltaan 6 cm x 6 cm, ja niiden hyötysuhde parhaimmillaan yli 3 %, mikä on jo lupaava arvo ottaen huomioon mm. vastaelektrodilla tapahtuvat, substraatin pintavastuksesta johtuvat ohmiset häviöt. Näiden häviöiden minimoimiseksi integroitiin vastaelektrodiin ylimääräiset virrankeräinrakenteet hopeananopartikkelimusteella mustesuihkutulostustekniikalla. Virrankeräinrakenteilla onnistuttiin pienentämään kennon kokonaisvastusta 50 % ja korvaamalla valoelektrodin lasisubstraatti RST:llä 80 %.

RST-pohjainen kenno vaikuttaisi toteuttamiskelpoiselta ratkaisulta jopa teollisen mittakaavan massatuotantoon, mutta erityistä huomiota tulisi jatkotutkimuksissa kehittää sen pitkän ajan stabiilisuuden parantamiseen. Myös hyötysuhdetta tulisi saada nostettua – tässä mm. hiilinanomateriaalit ovat eräs varteenotettava tutkimuskohde.

Asiasanat Väriaineherkistetty aurinkokenno, muovisubstraatti, metallisubstraatti, nanomateriaalit

ISBN (painettu) 978-952-60-3069-2	ISSN (painettu) 1795-2239
ISBN (pdf) 978-952-60-3070-8	ISSN (pdf) 1795-4584
Kieli Englanti	Sivumäärä 64 s. + liit. 91 s.

Julkaisija Aalto-yliopiston teknillinen korkeakoulu

Painetun väitöskirjan jakelu Teknillisen fysiikan laitos

☒ Luettavissa verkossa osoitteessa http://lib.tkk.fi/Diss/2010/isbn9789526030708/

Preface

This thesis is based on research carried out at the Helsinki University of Technology (TKK), Department of Applied Physics, at the New Energy Technologies group (NEW) between years 2004 - 2010. Funding for this work was provided mainly by Finnish Funding Agency for Technology and Innovation (Tekes) and Academy of Finland. I would also like to thank the Finnish Foundation for Technology Promotion (TES) for an incentive scholarship and the National Graduate School of Energy Technology for the travel grants for conference trips.

I thank my supervisor, professor Peter Lund for introducing me to the diverse and dynamic field of photovoltaics and especially to one of its latest inventions, nanostructured dye solar cell. Experimenting with this cell type calls for multidisciplinary approach, combining chemistry, physics and material science. As I came from quite a different field there has been a lot to learn and the road has been rocky at times but nothing truly valuable in this life comes easily.

What forms the core of an efficient, productive, encouraging, and pleasant workplace are people. This is why I have immensely enjoyed my years in the NEW group – not only because of the high academic quality of the research here but because of the friendly, relaxed and helpful working atmosphere. It was easy to integrate into this group straight from the beginning and there have been people who became not only workmates at the time but also good friends, expanding my horizons and introducing me to new and interesting things also outside of the academic world. My sincere thanks go to my current colleagues Dr. Janne Halme, Dr. Kati Miettunen, Kerttu Aitola, Suvi Karvonen, Rami Niemi, Imran Asghar, and Ghufran Hashmi, and all Master's Thesis and special assignment workers whose work contribution has been an important part of our research too. And all the former workmates – Dr. Mikko Mikkola, Dr. Petri Konttinen, Dr. Thomas Carlsson, Dr. Tero Hottinen, Dr. Olli Himanen, Dr. Iwao Nitta, Dr. Jukka Paatero, Dr. Marju Ferenets from Tampere Technical University, Timo Peltola, Saara Tuurala, Sonja Auvinen, Timo Lehtinen, Fredrik Ahlskog, Antti Tolvanen, Jaakko Saarinen – it was a pleasure to work with you. If I forgot someone, my sincere apologies – lots of people come and go in six years.

The international nature of this field, industrial co-operation and possibility to learn not only scientific but also organizational and teaching skills have also been extremely valuable dimensions of my job here.

Finally, sincere thanks to my parents, Eila and Kalevi Toivola, for your endless support in everything I've ventured to in my life, and to my friends, for providing pastime and entertainment definitely non-academic by nature.

Otaniemi, Espoo, February 2010

Minna Toivola

Table of contents

List of Publications

I Halme, Janne; **Toivola, Minna**; Tolvanen, Antti; Lund, Peter, *Charge transfer resistance of spray deposited and compressed counter electrodes for dye-sensitized nanoparticle solar cells on plastic substrates*, Solar Energy Materials and Solar Cells 90, 872-886 (2006). http://dx.doi.org/10.1016/j.solmat.2005.05.007

II **Toivola, Minna**; Ahlskog, Fredrik; Lund, Peter, *Industrial sheet metals for nanocrystalline dye-sensitized solar cell structures*, Solar Energy Materials and Solar Cells 90, 2881-2893 (2006). http://dx.doi.org/10.1016/j.solmat.2006.05.002

III **Toivola, Minna**; Peltokorpi, Lauri; Halme, Janne; Lund, Peter, *Regenerative effects by temperature variations in dye-sensitized solar cells*, Solar Energy Materials and Solar Cells 91, 1733-1742 (2007). http://dx.doi.org/10.1016/j.solmat.2007.05.030

IV **Toivola, Minna**; Halme, Janne; Peltokorpi, Lauri; Lund, Peter, *Investigation of temperature and aging effects in nanostructured dye solar cells studied by electrochemical impedance spectroscopy*, International Journal of Photoenergy 2009, Article ID 786429 (2009). http://dx.doi.org/10.1155/2009/786429

V Miettunen, Kati; Halme, Janne; **Toivola, Minna**; Lund, Peter, *Initial performance of dye solar cells on stainless steel substrates*, Journal of Physical Chemistry C 112, 4011-4017 (2008). http://dx.doi.org/10.1021/jp7112957

VI **Toivola, Minna**; Peltola, Timo; Miettunen, Kati; Halme, Janne; Lund, Peter, *Thin film nano solar cells - from device optimization to upscaling*, Journal of Nanoscience and Nanotechnology 10, 1-7 (2010). http://dx.doi.org/10.1166/jnn.2010.1872

VII **Toivola, Minna**; Miettunen, Kati; Halme, Janne; Lund, Peter, *Thin Nanostructured Solar Cells on Metal Sheets*, NSTI Nanotech - The Nanotechnology Conference and Trade Show, Boston, U.S.A, June 1-5, 2008, Technical Proceedings of the CTSI Clean Technology and Sustainable Industries Conference and Trade Show, 96-99 (2008).

VIII **Toivola, Minna**; Ferenets, Marju; Lund, Peter; Harlin, Ali, *Photovoltaic fiber*, Thin Solid Films 517, 2799-2802 (2009). http://dx.doi.org/10.1016/j.tsf.2008.11.057

Author's contribution

I The author conducted the most of the experiments and data analysis and took part in writing the paper.

II The author planned the research, took part in the sample preparation, measurements and data analysis and wrote the most of the paper (based on the results reported in the M.Sc. thesis of Fredrik Ahlskog, which she supervised).

III The author planned the research, took part in the sample preparation, measurements and data analysis and wrote the most of the paper.

IV The author planned the research, took part in the sample preparation, measurements and data analysis and wrote the most of the paper.

V The author contributed to discussions about the paper with the co-authors and commented and proofread the paper, which is direct continuation to the research she initiated in Publication II.

VI The author planned the research, assisted in the measurements and data analysis and wrote the most of the paper (based on the results reported in the M.Sc. thesis of Timo Peltola, which she supervised).

VII The author wrote the most of the paper, which is a summary and overview of her own and her co-authors' work, some of which she partially supervised (M.Sc. thesis of Kati Miettunen).

VIII The author planned the research, developed a new material used in the samples, was mainly responsible for the sample preparation, measurements and data analysis and wrote the paper together with Marju Ferenets.

Other publications by the author not included in this thesis

Toivola, Minna; Halme, Janne; Miettunen, Kati; Aitola, Kerttu; Lund, Peter, *Nanostructured dye solar cells on flexible substrates - Review*, International Journal of Energy Research 33, 1145-1160 (2009). http://dx.doi.org/10.1002/er.1605

Miettunen, Kati; Halme, Janne; Vahermaa, Paula; Saukkonen, Tapio; Toivola, Minna; Lund, Peter, *Dye solar cells on ITO-PET substrate with TiO_2 recombination blocking layers*, Journal of The Electrochemical Society 156, B876-B883 (2009). http://dx.doi.org/10.1149/1.3138129

Miettunen, Kati; Halme, Janne; Saukkonen, Tapio; Peltola, Timo; Toivola, Minna; Lund Peter, *Performance degradation of dye solar cells on flexible stainless steel substrates*, 24th European Photovoltaic Solar Energy Conference, Hamburg, Germany, September 21-25, 2009, Proceedings of the 24th European Photovoltaic Solar Energy Conference, xxxx-xxxx (2009).

Asghar, Muhammad Imran; Miettunen, Kati; Halme, Janne; Toivola, Minna; Aitola, Kerttu; Vahermaa, Paula; Lund, Peter, *Stability issues of improved dye sensitized solar cells*, 24th European Photovoltaic Solar Energy Conference, Hamburg, Germany, September 21-25, 2009, Proceedings of the 24th European Photovoltaic Solar Energy Conference, xxxx-xxxx (2009).

Toivola, Minna; Peltola, Timo; Miettunen, Kati; Halme, Janne; Aitola, Kerttu; Lund, Peter, *Large area optimized thin film nano solar cells on metal sheet*, NSTI Nanotech – The Nanotechnology Conference and Trade Show, Houston, U.S.A, May 3-7, 2009, Technical Proceedings of the CTSI Clean Technology and Sustainable Industries Conference and Trade Show, 126-129 (2009).

Guangseng, Huang; Halme, Janne; Miettunen, Kati; Toivola, Minna; Lund, Peter, *The performance enchancement by back reflection in nanostructured dye-sensitized solar cells*, ISES World Congress 2007, Beijing, China, September 18-21, 2007, Proceedings of the ISES World Congress, 1055-1058 (2007).

Toivola, Minna; Halme, Janne; Peltokorpi, Lauri; Lund, Peter, *Aging and regenerative behavior through cyclic temperature of nanostructured, dye-sensitized solar cells*, 22nd European Photovoltaic Solar Energy Conference, Milan, Italy, September 3-7, 2007, Proceedings of the 22nd European Photovoltaic Solar Energy Conference, 454-460 (2007).

Miettunen, Kati; Toivola, Minna; Halme, Janne; Armentia, Jon; Vahermaa, Paula; Lund, Peter, *Optimization of dye-sensitized solar cells on stainless steel*, 22nd European Photovoltaic Solar Energy Conference, Milan, Italy, September 3-7, 2007, Proceedings of the 22nd European Photovoltaic Solar Energy Conference, 512-515 (2007).

Toivola, Minna; Miettunen, Kati; Halme, Janne; Ahlskog, Fredrik; Lund, Peter, *Nanostructured dye-sensitized solar cells on flexible substrates using industrially scaleable manufacturing methods*, 21st European Photovoltaic Solar Energy Conference, Dresden, Germany, September 4-8 , 2006, Proceedings of the 21st European Photovoltaic Solar Energy Conference, 47-52 (2006).

Abbreviations

AC	alternating current
AM 1.5 G	incident air mass 1.5 global spectrum
a-Si	amorphous silicon
BIPV	building-integrated photovoltaics
CE	counter electrode
CIGS	copper-indium-gallium selenide
CIS	copper-indium sulphide
CPE	constant phase element
DMPII	1,2-dimethylimidazolium iodide
DSC	dye-sensitized solar cell
EIS	electrochemical impedance spectroscopy
EPIA	European Photovoltaic Industry Association
FTO	fluorine-doped tin oxide
HOMO	highest occupied molecular orbital
IR	infrared
ITO	indium-doped tin oxide
LED	light-emitting diode
LUMO	lowest unoccupied molecular orbital
MePRN	3-methoxypropionitrile
PANI	polyaniline
PE	photoelectrode
PEDOT	poly(3,4-ethylenedioxythiophene)
PEN	polyethylenenaphtalate
PET	polyethyleneterephtalate
PMII	1-methyl-3-propylimidazolium iodide
PMMA	polymethylmethacrylate
PV	photovoltaic
PVDF-HFP	polyvinylidenefluoride-hexafluoropropylene
spiro-MeOTAD	2,2′7,7′-tetrakis-(N,N-di-p-methoxyphenyl-amine)-9,9′-spirobifluorene
StS	stainless steel
TCO	transparent conducting oxide
TL	transmission line
UV	ultraviolet

Symbols

B_0	CPE impedance pre-factor
C	capacitance
C_{ce}	CE capacitance
c_{I3-}	triiodide concentration
C_{pe}	PE capacitance
CPE_{ce}	CPE describing the CE capacitance
CPE_{co}	CPE describing the capacitance at the substrate-TiO_2 interface
CPE_{pe}	CPE describing the PE capacitance
cpe_{pe}	distributed PE CPE element
CPE_{su}	CPE describing the capacitance at the substrate-electrolyte interface
d	TiO_2 film thickness
D_{I3-}	triiodide diffusion coefficient
F	Faraday's constant
f	frequency
f^*	characteristic frequency
FF	fill factor
h	Planck's constant
I_{AC}	AC current signal in EIS
I_d	diode current
i_{lim}	diffusion-limited current density
I_{mpp}	current at maximum power point
I_{ph}	photogenerated current
$I_{ref,sim}$	current of a reference cell in a solar simulator
$I_{ref,std}$	current of a reference cell under standard spectrum
I_{sc}	short circuit current
$I_{test,sim}$	current of a measured cell in a solar simulator
$I_{test,std}$	current of a measured cell under standard spectrum
l	distance between electrodes
L_e	electron diffusion length
M	spectral mismatch factor
n	number of electrons transferred in a reaction
P_{in}	power of incident light
R	resistance
R_{ce}	charge transfer resistance at the CE
R_{co}	resistance at the substrate-TiO_2 interface
R_{pe}	PE resistance
r_{rec}	distributed recombination resistance element
R_{rec}	electron recombination resistance at the PE
R_s	series resistance
R_{su}	resistance at the substrate-electrolyte interface
r_{tr}	distributed transport resistance element

R_{tr}	electron transport resistance in the PE film
V_{AC}	AC voltage signal in EIS
V_{mpp}	voltage at maximum power point
V_{oc}	open circuit voltage
Z	impedance
Z'	real impedance
Z''	imaginary impedance
Z_{CPE}	CPE impedance
Z_d	diffusion impedance
β	CPE impedance exponent
η	power conversion efficiency
ν	photon's frequency
τ_e	electron lifetime
ω	angular frequency

1 Introduction

1.1 Background

Depletion of easily utilizable fossil fuels in near future, along with the threat of global warming, which may be partially a result of constantly growing greenhouse gas emissions in energy production have made research, development and implementation of renewable energy one of the most crucial challenges of today's mankind. This is accentuated by the massive industrialization that is behind the rapid economical growth in countries such as China and India, and the drive towards Western standards of living in the developing world. In these countries, the constantly increasing energy consumption is still typically covered with cheap and highly polluting methods such as burning coal. Ecological awareness and the legislation concerning the environmental aspects of industrial activity in these parts of the world also tend to lack behind the Western, especially European standards. The reserves of fossil and even nuclear fuel are also limited – for example, the constantly growing gas prices give indication that the exhaustion of crude oil is maybe not so far in the future anymore than always thought. Also, despite the tight safety regulations and procedures in modern nuclear power plants nuclear energy still raises lots of opposition amongst the consumers.

The technologies to utilize the enormous energy potential that lies in the Sun have existed for several decades already but the still high price of the photovoltaic (PV) panels and the current PV devices' suitability for only limited variety of applications have hindered solar power's large scale usage. This is why development of new, more advanced, cheaper and efficient solar energy technologies is called for to bring this form of renewable energy available to even larger number of customers.

1.2 Objectives of the study

This study concentrates on dye solar cells (DSC) [1-4], which represent the so-called third generation of photovoltaics – crystalline silicon being the first, and thin film technologies such as cadmium telluride (CdTe), copper-indium-gallium selenide (CIGS), copper-indium sulphide (CIS) and amorphous silicon (*a*-Si) being examples of the second generation. Introduced in the early 90's, DSC is still a relatively new concept in the field of PV, considering the first crystalline silicon solar cells were manufactured already in the 50's. Unlike the conventional, solid semiconductor solar cells (1st and 2nd generation), the DSC is a photoelectrochemical device which operating principle mimics the photosynthesis reaction of the green plants. The advantages of this technology lie in its simple and energy-efficient manufacturing, for the most part low cost, non-toxic and recyclable materials, and suitability for wide variety of end-user products, from small scale power production to consumer goods such as mobile phone chargers or "smart" clothing. Also, as the DSC works better with low light intensities it is especially practical in indoor applications.

The main hindrances of the breakthrough of the DSC technology are the cells' still somewhat low power conversion efficiency, uncertainties considering the cells' long term stability, and the fact that the best DSCs are still prepared on fragile and inflexible glass substrates suitable only for batch process manufacturing. The best DSC efficiencies measured in the laboratory exceed already 10-11 % at the moment with carefully optimized cell configuration [5-7], which is comparable to the values typical for thin film technologies (5 – 13 %) but still lack behind the crystalline silicon values which are already almost 20 % [8]. However, as the DSC can also be prepared on flexible, non-fragile and light weight substrates such as plastic foils or metal sheets and with simple and well established methods familiar to e.g. coating and printing industries, it enables high throughput, cost-efficient roll to roll type production of the cells. Indeed, the potentially low cell price which follows from fast, large scale mass production makes manufacturing of even lower efficiency and lower lifetime DSC devices economically feasible.

This thesis is experimental by nature and its main objective was to study alternative dye solar cell substrates to glass, namely ITO-PET (indium-doped tin oxide coated polyethyleneterephtalate) plastics and industrial sheet metals. In comparison to the typical planar cell geometry, integration of the DSC on optical fibers was also investigated. Enlarging of the plastic/metal-based DSC from small, laboratory-size test cells to industrially upscaleable "mini-modules" was an integral part of the research and, as the operating conditions of the cells vary according to ambient weather and the geographical location of the panels, preliminary studies on the effect of temperature on the cell function and long-term stability are also included.

1.3 Thesis outline

The outline of this thesis is as follows:

Chapter 1 presents the background and the main objectives of the study.

Chapter 2 describes the principles behind the operation of PV devices, especially those of the DSC, and discusses the state-of-the-art in DSC research. DSC materials and manufacturing methods are introduced and special emphasis is put on alternative substrates to glass.

Chapter 3 presents the research methods and measurement techniques used in the study.

Chapter 4 describes the experimental part of the study, i.e. cell preparation, measurements and data analysis.

Chapter 5 gives a summary and overview of the results, reported originally in Publications I – VIII. The results are discussed and compared to previous scientific findings in the field.

Chapter 6 consists of more general conclusions and discussion of the topic and Chapter 7 lists the references used in this study.

2 Dye-sensitized solar cells (DSC)

2.1 Background, motivation and current status of solar energy utilization

Of all renewable energy sources, solar power is one of the most easily exploitable, endlessly and constantly abundant, silent, and adaptable to wide variety of applications from several hundred MW outdoor power plants that produce both heat and electricity [9] to small off-grid systems that can power areas of rural settlement and dispersed development. In addition to their basic function which is energy production, the latter applications can also have big social impact on areas such as Africa, where big parts of the population still live in primitive conditions and extreme poverty. For example, solar-powered fridges enable transport and storage of vaccines and drugs in hot climate and solar cookers can replace open fires that typically consume large amounts of wood which collection both works in favor of desertification and keeps women tied to household chores. In houses, solar-powered LED (light-emitting diode) lights can replace inefficient and toxic kerosene lamps traditionally used for illumination, thus providing properly lit environment for example for children to study. On even smaller scale and especially with the new, flexible PV technologies, solar energy can also be used to run low-power consumer electronics such as laptop computers and mobile phones or it can be integrated to textiles. These "intelligent", power-generating garments are an interesting approach especially from the viewpoint of military and camping equipment manufacturers and can be utilized in vital function monitoring systems which are used in e.g. hospitals and geriatric/disabled people care units. Some solar cell types can also be directly integrated on building materials, thus realizing products such as electricity-generating roofings and facades, or, due to their transparency, be used as partially shadowing windows that at the same time produce power to the indoor functions of the house. The constantly expanding field of printed electronics also benefits from thin, flexible solar cells that can be manufactured with the same techniques as the main devices.

To private customers, PV's viability and attractiveness lie in the systems' low need for maintenance and silent operation, the constantly increasing lifetime of the PV panels (current estimate being already 30 years [8]) and at the same time lowering prices, and the system reliability: the system efficiency stays well within 80 % of the initial value the whole lifetime of the product, which is why the energy payback time may be as low as only a few years [8]. As solar energy is produced locally, it also increases energy independence and creates jobs. Even in countries where sun conditions are not ideal, like Finland, utilizing solar power works as an energy saving procedure and technological know-how related to the topic can be an important export product in the future.

The total amount of solar radiation intercepting Earth is approximately 174 PW (Figure 1), which is over 10 000 times the entire global energy consumption [9]. Also, the area that needs to be covered with solar panels to power the whole Earth is no more than 100 000 km^2 – only one third of the land area of Finland. Or, to produce electricity to whole Europe, only 2 % of the continent's land area needs to be covered with PV panels

[8]. These figures give indication of the enormous potential that lies in the Sun, even if practical issues such as transporting the power with minimal losses or finding big enough continuous land areas in climates optimal for solar energy production for large scale power plants obviously set limitations to its full scale utilization.

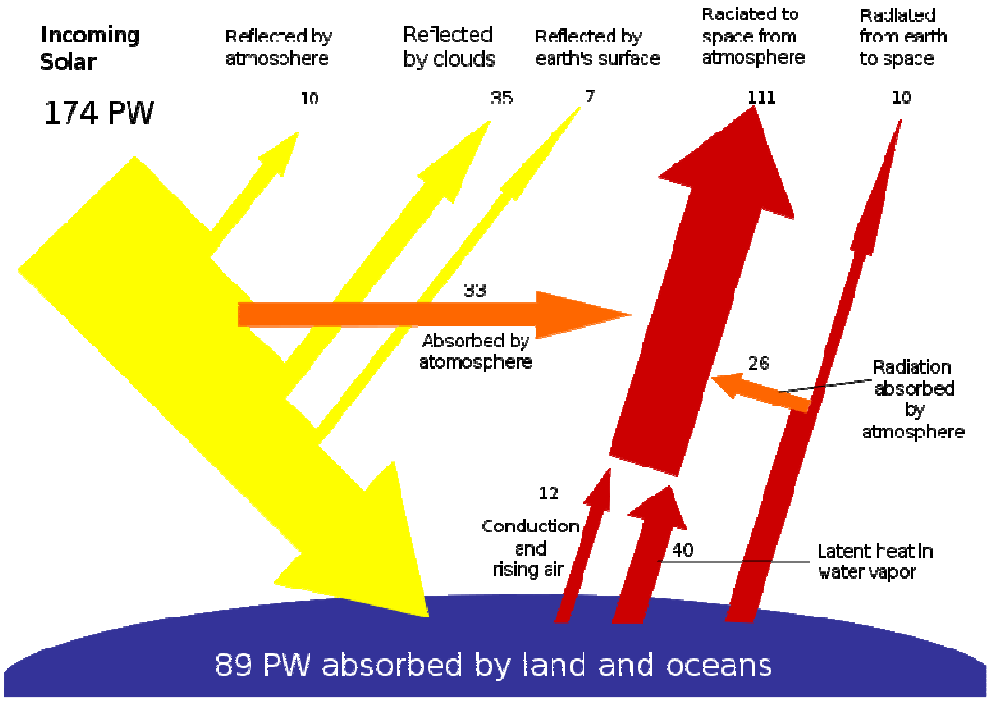

Figure 1. Solar energy intercepting Earth [9].

When compared to the traditional, fossil fuel based energy production, solar power is still somewhat marginal phenomenon, contributing to the global energy usage by only 0.54 % [9]. Of this, the predominant part is solar heat and only 0.04 % solar electricity, the cumulative total of installed PV being ca. 9 GW up to this day [8, 9]. However, the average annual market growth of the photovoltaic industry has been 35 – 40 % for several years already, and, for example 2007, grid-connected PV was the fastest growing source of energy with its 83 % increase [9]. The current leaders in photovoltaics are Spain and Germany which, according to 2008 statistics, contributed to the 6 GW total of PV installed globally that year with 2.46 GW and 1.86 GW, respectively (Figure 2) [10]. The market growth was impressive especially in Spain: 285 % from the previous year [10]. These numbers, along with the constantly increasing production capacity of solar panels (doubling every two years [9]), lowering costs and technological advancements in panel efficiency and long-term stability, show that despite its reputation of being a niche energy source, solar power is an attractive and profitable investment which has even been proposed as the most likely replacement for fossil fuels in the future. Oil, gas, and coal might never be completely exhausted, but their utilization becomes more and more

difficult and expensive in the near future, which has made even the big oil companies such as Shell and BP to invest large sums in solar energy research [11, 12].

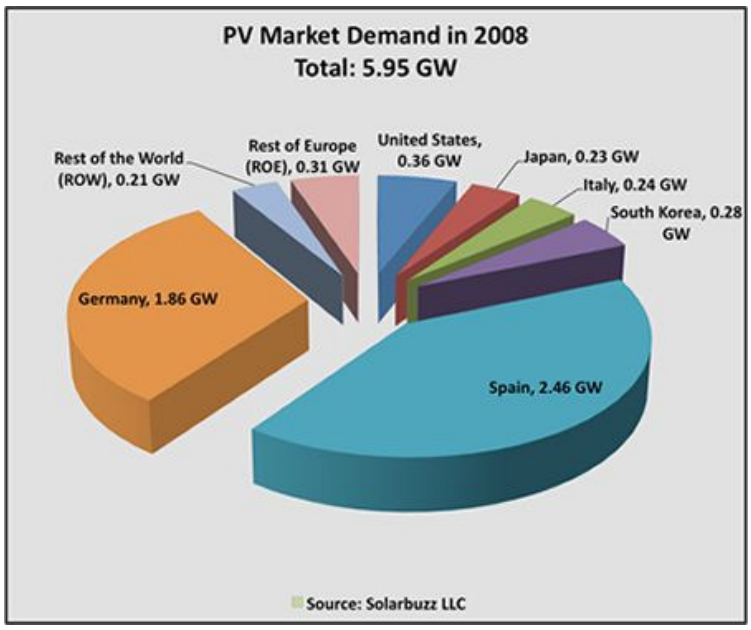

Figure 2. Distribution of PV installed globally in 2008 [10].

Even if the PV technologies are well established and the modern solar power systems are relatively easy to install it still needs political will to make solar energy profitable to a common customer. The success of especially Germany in solar energy utilization lies in its feed-in tariff system, in which the consumers are able to sell the electricity produced by their PV panels back to the electricity company, and with higher price than the price of the regular grid electricity, which shortens the PV system payback time considerably. Similar systems exist also in Spain, Italy, France and Greece [8].

Despite the constantly lowering manufacturing costs of the PV panels, the main problem in the breakthrough of solar power is its still high price compared to grid electricity – for example, EPIA (European Photovoltaic Industry Association) predicts that it will take at least ten years still until PV will become truly economically competitive with conventional grid power in Europe [8]. One of the reasons for this is the difficult and energy intensive manufacturing process of silicon solar panels which still contribute to all installed PV with 90 % [8]. Shortage of ultra-pure solar grade silicon may also loom in the future, as also the microchip and sensor industries consume large amounts of this raw material. Traditional silicon PV panels are also heavy, inflexible, suitable for only limited number of applications and usually protected by glass sheets which may break easily. New technologies are thus called for to realize more economically feasible, large scale utilization of solar energy.

2.2 Principles of photovoltaic conversion

All photovoltaic energy conversion is based on photoelectric effect, in which light falling on (semiconductor or other) material creates an electron-hole pair in it (Figure 3). To extract electricity out of the system, the electrons and holes must be separated before recombination, after which they can be transferred to an external circuit. How this charge carrier separation is realized, depends on the solar cell type.

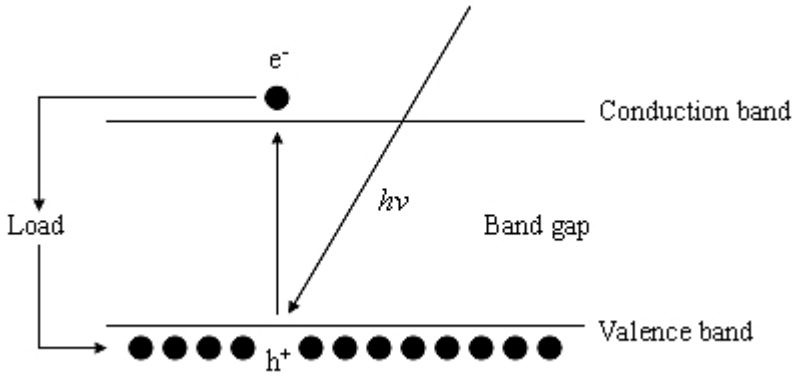

Figure 3. Electron-hole pair generation in a semiconductor.

In conventional, solid semiconductor solar cells, electrons and holes are driven apart by internal electric field in the device. This field forms around the *p-n* junction, which is the core of all solid semiconductor photovoltaics. *P-n* junction is created by combining blocks of oppositely doped semiconductors, for example silicon doped with boron and silicon doped with phosphorus. The former is called *p*-type silicon, due to boron's valency of three, which is one electron less than that of silicon's and thus results in electron depletion (positive "holes") in silicon's valence band. Analogously, the latter is called *n*-type silicon, due to phosphorus' valency of five, which results in excess electrons on silicon's conduction band. When these blocks are brought to physical contact, the "extra" electrons in the *n*-type silicon flow to fill the "holes" in the *p*-type silicon, thus leaving behind ionized dopant atoms, as well as creating those in the *p*-side, when boron's valency of three exceeds by one. These ionized dopants then create the internal electric field that affects in the so-called depletion region around the *p-n* junction. When an electron-hole pair is generated in this region, the internal electric field sweeps the charge carriers on the opposite sides of the junction, thus preventing recombination (Figure 4).

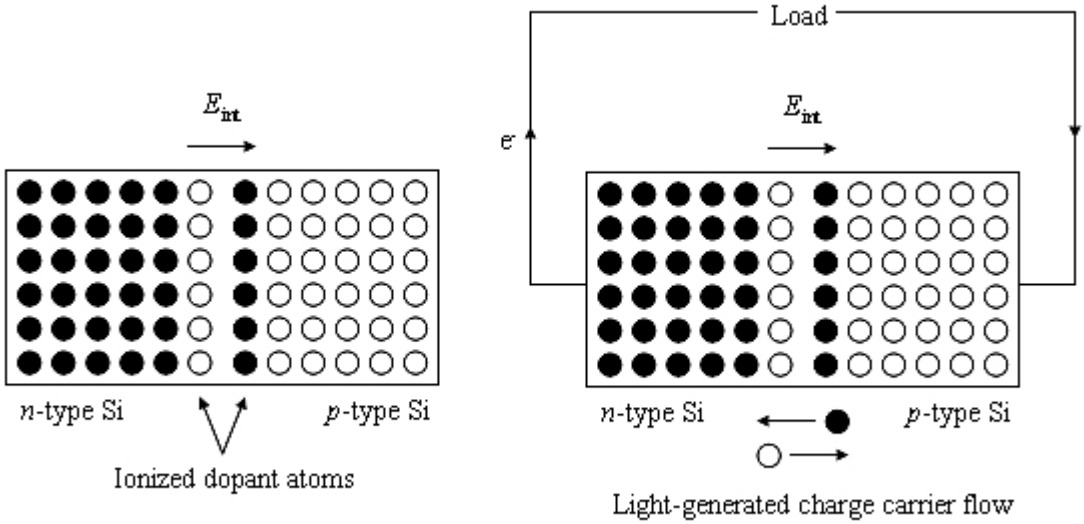

Figure 4. A *p-n* junction in dark (left) and in light (right). E_{int} = internal electric field. The black circles symbolize net negative charge, the white circles net positive charge.

Energetically, the same can be understood by "bending" of the valence and conduction bands. In an undoped semiconductor, the Fermi level is located in the middle of the band gap. When the semiconductor is doped with atoms with "extra" electrons, the Fermi level shifts upwards and analogously, when the dopant causes electron depletion, the Fermi level moves lower. When the oppositely doped blocks are brought to contact, the flow of electrons from the *n*-side to the *p*-side shifts the *n*-side conduction band lower and correspondingly, the flow of holes from the *p*-side to the *n*-side moves the *p*-side valence band higher on electronic energy scale. As a result of this, the Fermi levels match throughout the junction. Because of this band "bending", it is energetically favorable for the photogenerated charge carriers to move across the junction, i.e. electrons created on the *p*-side flow "downwards" to the *n*-side and holes created in the *n*-side move "upwards" to the *p*-side. Typically, either *n*- or *p*-side is doped heavier so the depletion region reaches further in this side and the most of the charge carriers can be collected there. This offers also the benefit that the junction itself can be brought close to the solar cell surface, thus maximizing the amount of absorbed photons.

In DSC, the charge carrier separation happens on an interface between electronic and ionic conductors (Figure 5). The semiconductor typically used in these cells, titanium dioxide, has band gap too wide for visible light to evoke photoelectric effect, but the electrons are fed into the material from electronically excited dye molecules adsorbed on its surface. In this process, the dye gets oxidized, i.e. a positive charge is created. For the electron injection process to continue the dye needs to be reduced back to its ground state, which is done by electrolyte which contains a redox couple and is in contact with the TiO_2 layer. Thus, the positive "hole" is transferred into the electrolyte as the oxidized form of the redox couple and the electrons are fed into the TiO_2. Because the holes can

not move in the TiO_2 and electrons in the electrolyte, charge carrier separation is achieved. The electron injection from the dye to the TiO_2 is energetically favorable because the excited electronic state of the dye is located slightly higher than the TiO_2 conduction band. The injection process is also several decades faster than the competing reactions, i.e. relaxation of the dye back to the ground state or recombination (the details of the charge transfer processes in the DSC are discussed in more detail in Chapter 2.3).

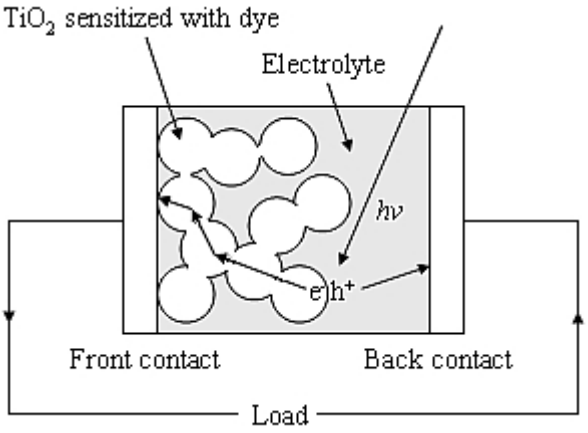

Figure 5. Charge carrier separation in the DSC.

2.3 DSC structure and operating principle

The DSC differs from other solar cells types both by its basic construction and the physical processes behind its operation. Unlike the 1st and 2nd generation PV devices based on solid semiconductor materials, the typical DSC configuration combines solid and liquid phases. Electricity is generated on the photoelectrode, which is a nanoporous TiO_2 film sensitized with a monolayer of visible light absorbing dye and penetrated with a redox electrolyte. The TiO_2-electrolyte network is sandwiched between two conductive substrates that also work as current collectors. The opposite substrate to the TiO_2 layer, the counter electrode, is coated with a material capable of catalyzing the redox reaction in the electrolyte. Thus, the DSC resembles more an electrochemical cell than a conventional *p-n* junction solar cell.

Research on wide band gap oxide semiconductors sensitized with dyes began already in the late 1800's, related to photography. The first studies on dye-sensitized TiO_2 and ZnO photoelectrodes were done in 1960's and 1970's, but due to a limited amount of dye that could be adsorbed on macrocrystalline semiconductors and too narrow spectral absorbance range of the dyes the photocurrent and cell efficiency stayed on very modest level [3]. Improvement to this was achieved in the early 1990's, thanks to nanotechnology and development of better dyes. Nanocrystalline TiO_2 enabled drastic multiplying of the effective surface area of the photoelectrode for the dye to adsorb, and

the new ruthenium bipyridyl organometallic complexes (Figure 6) had absorbance range from visible to near-infrared wavelengths [3].

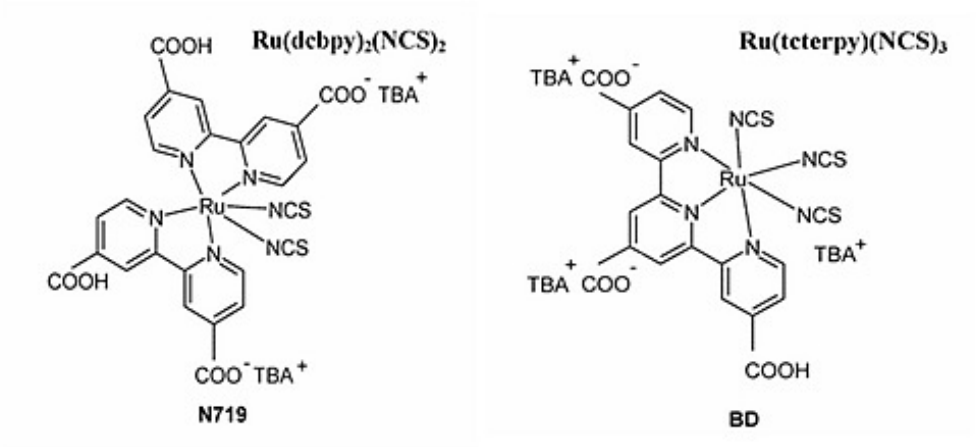

Figure 6. Molecular structures of some common dyes, the so-called N-719 and "black dye" (BD) [3].

The basic DSC structure and operating principle are presented in Figure 7. Photon absorption induces a metal-to-ligand type electronic transition between the HOMO (highest occupied molecular orbital) and LUMO (lowest unoccupied molecular orbital) of the dye. Since the LUMO is located in the vicinity of the ligands (pyridyl π-orbitals) the electron injection to the TiO_2 is spatially favorable. Efficient electron injection is further enhanced by the strong electronic interaction that forms when the dye bonds to the TiO_2 with the ligand carboxyl groups (Figure 8) and the energetic location of the TiO_2 conduction band in relation to the LUMO of the dye (Figure 9). Efficient charge separation is, on the other hand, achieved because the electrons and holes travel in different mediums – this prevents bulk recombination which is a problem in conventional *p-n* junction cells. The competing reactions, i.e. recombination of the photogenerated electrons with the oxidized form of the dye or the redox species in the electrolyte (Figure 10; the latter reaction referred to as "dark current" in the picture) proceed also several decades slower than the electron injection process. In addition to that, the electrolyte cations and protons released in the dye adsorption process intercalate to the TiO_2 surface and lattice where they, together with the negative species in the electrolyte, form a Helmholtz dipole layer on the photoelectrode surface. This enhances charge separation even further.

The amount of current that the cell is able to generate is determined by the energetic distance of the HOMO and LUMO of the dye, which equals the band gap in inorganic semiconductors. The maximum voltage, on the other hand, is defined as the difference between the redox level of the electrolyte and the Fermi level of the TiO_2 (Figure 9). With iodide/triiodide redox couple, this difference is ca. 0.9 V, though slight variation is caused by the electrolyte composition due to species adsorbed on the TiO_2 surface, which

may alter the Fermi level position somewhat. Also, there is always some recombination in the cell which lessens the amount of electrons in the TiO_2 film, thus lowering the Fermi level and decreasing the cell voltage.

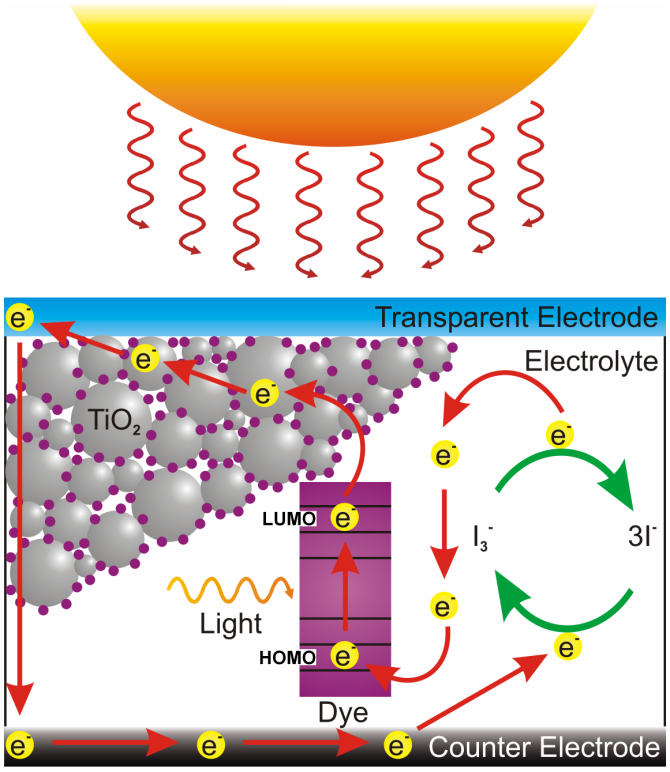

Figure 7. The structure and operating principle of the DSC. Modified from the picture presented in [13].

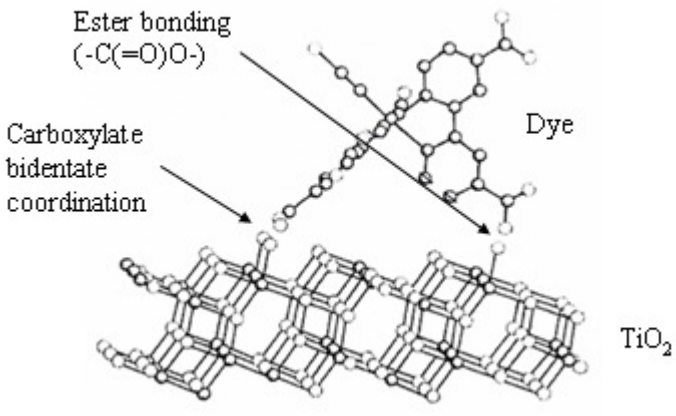

Figure 8. Dye bonding to the TiO_2. Two possible bonding mechanisms (ester bonding and carboxylate bidentate coordination) presented. Modified from a picture from [3].

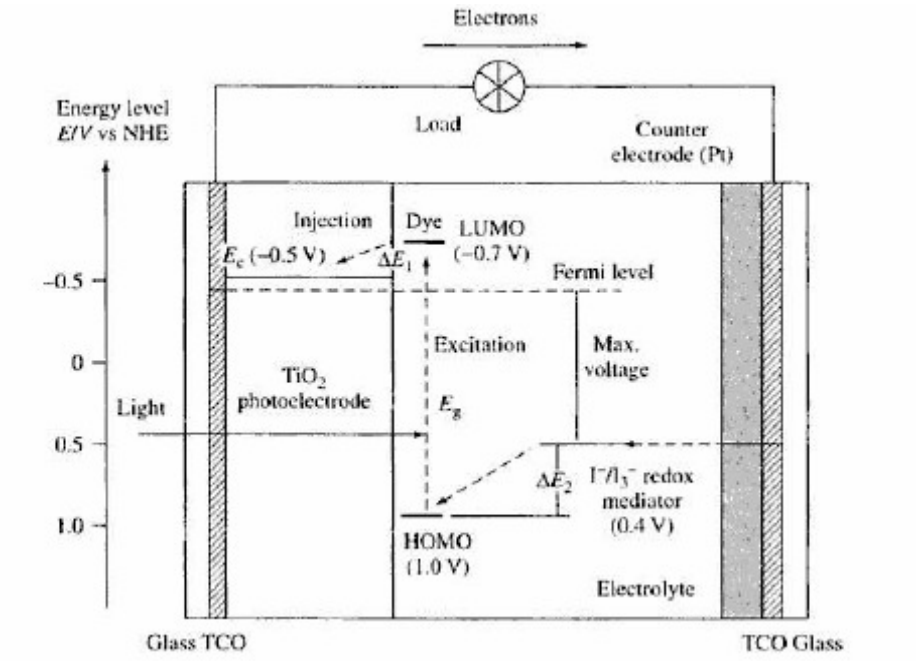

Figure 9. The energy level scheme of the DSC [3].

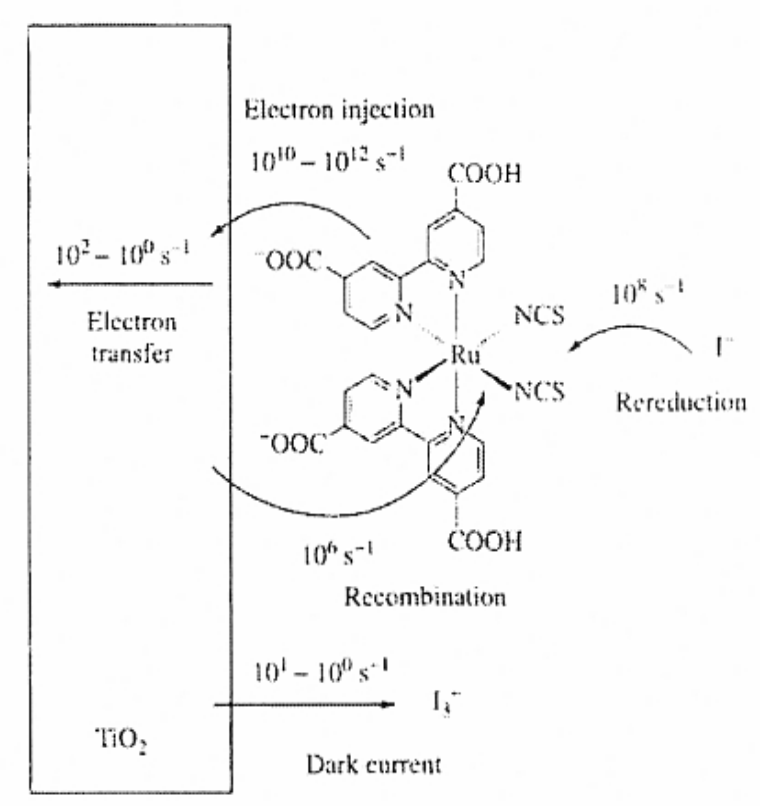

Figure 10. The electron transfer reactions and their timescales in the dye-TiO_2-electrolyte system [3].

After injection, electrons diffuse in the nanocrystalline TiO_2 network to the conductive coating of the substrate, from which they can be transferred to an external circuit. There exist various models for the electron diffusion in the TiO_2 film but thermally activated trapping/detrapping mechanism along localized energy levels below the TiO_2 conduction band edge seems the most realistic one, in the light of experimental evidence [14-17]. The electron injection to the TiO_2 leaves the dye molecule on an oxidized state so, in order for the current generation to continue, the dye must be reduced back to its ground state. This is done by the redox couple in the electrolyte. The most commonly used redox couple, and the one that gives the best cell efficiencies when combined with TiO_2, is iodide/triiodide. The oxidized dye gets electrons from the iodide ions which, in turn, get oxidized to triiodide in the process. The triiodide ions then diffuse to the counter electrode, where they get reduced back to iodide by the electrons returning from the external load. Thus, the cell operation is based on consecutive reduction/oxidation cycles and, in an ideal cell, no chemical substances are permanently transmuted. The most often used counter electrode catalyst for the triiodide/iodide reduction reaction is platinum, though also carbon materials and certain conductive polymers have been successfully employed in this function [18].

The chemical reactions going on in the cell can be summarized as follows:

At the photoelectrode (S^0 = the ground state of the dye; S^* = the excited state of the dye; S^+ = the oxidized state of the dye):

- Light absorption: $2S^0 + 2h\nu \rightarrow 2S^*$ (1)
- Electron injection: $2S^* \rightarrow 2S^+ + 2e^-(TiO_2)$ (2)
- Dye reduction and iodide oxidation: $2S^+ + 3I^- \rightarrow 2S^0 + I_3^-$ (3)
- Overall: $3I^- + 2h\nu \rightarrow I_3^- + 2e^-(TiO_2)$ (4)

At the counter electrode:

- Triiodide reduction: $I_3^- + 2e^- \rightarrow 3I^-$ (5)

2.4 DSC basic materials and manufacturing methods

2.4.1 Substrates

Requirements for a good DSC substrate are low sheet resistance which should also be independent of temperature up to 450 – 500 ^{o}C (in case when the electrode post-treatment requires sintering), high transparency, and ability to prevent impurities such as water and oxygen from entering into the cell. The traditional approach is to build the DSC on transparent conducting oxide (TCO) coated glass sheets. The most often used TCOs are fluorine- and indium-doped tin oxides, whose sheet resistances are around 10 Ω/□. Whilst glass is obviously an effective barrier towards water and oxygen penetration into the cell, its disadvantages are fragility, rigidity, heavy weight and high price. ITO's sheet resistance also increases with temperature so ITO-coated glass is not the best option for cells where high temperature treatments are needed.

Alternative substrate materials such as plastic foils and metal sheets overcome most of the glass' problems. Conductive plastics, like ITO-PET and ITO-PEN (indium-doped tin oxide coated polyethylenenaphtalate), are light weight and flexible, whereas metals are also mechanically robust, cheap, and their electrical conductivity is superior compared to all other substrate materials. The last factor plays a crucial role in cell size upscaling, since the main part of the total ohmic losses in the cell are due to lateral resistance on the substrate surface. It has also been noticed that substrate-mediated recombination is lower from stainless steel than from glass [19]. Disadvantages of plastics include low temperature tolerance, max. 150 – 160 ^{o}C, for ITO-PET high sheet resistance, around 60 Ω/□, and uncertainties considering the oxygen and water penetration. For metals, the main problem is the traditionally used, iodine-containing electrolyte. Triiodide ions are corrosive, and thus far only stainless steel and titanium have shown enough chemical stability in the iodine electrolyte to be successfully employed as DSC substrates [19-27]. Long-term stability of metal-based cells is still unknown, though, and requires further studies before this DSC type can be transferred to large scale manufacturing. However, the main spur behind the alternative substrate research is the flexibility of both the plastic and metal substrates which enables roll-to-roll type manufacturing of the DSC, potentially leading to high volume production of low cost solar cells with wide variety of applications.

2.4.2 Photoelectrode

The semiconductor material that forms the core of the photoelectrode (PE) should be chemically stable and inert towards the electrolyte species, it should have a lattice structure suitable for dye bonding, its conduction band should be located slightly below the LUMO level of the dye in order to facilitate efficient electron injection, and it should be available in nanostructured form to enable high enough dye loading. Titanium dioxide fulfills these requirements – in addition to that, it is also cheap and easily available

because of mass production. The material is in wide use for example in pigments and paints and, due to its non-toxicity, even in cosmetic, hygiene and food products. Another semiconductor oxide that has been employed in the DSC is zinc oxide but there have been problems for example with the dye desorption [28] which is why TiO_2 is still the most widely used DSC photoelectrode material.

TiO_2 exists in three crystalline forms, anatase, rutile, and brookite, of which the anatase structure is the most suitable for DSC applications. The typical TiO_2 nanoparticle size in the PE film is 10 – 30 nm, though larger particles up to 300 – 400 nm are sometimes added to the film to increase the path length of the absorbed photons by scattering (improved light harvesting efficiency). The optimal PE film thickness is 10 – 15 µm – if the film is very thin the dye loading remains too low whereas with too thick films, the distance the excited electrons generated on the electrolyte side of the PE film have to travel before reaching the current collector becomes so long that increased recombination probability starts to decrease the cell efficiency.

Screen-printing is a typical TiO_2 layer deposition method, with which large quantities of even quality films can be prepared with high speed (on laboratory scale, technique called "doctor-blading", in which the TiO_2 precursor is applied through a hand-cut tape mask is often employed). Several research groups prepare their own TiO_2 precursor materials but there exists also commercial titania pastes specifically designed for screen-printing technique – in addition to the TiO_2 nanoparticles they contain some high viscosity organic solvent, binders, pH-adjusting agents, and morphology controlling agents. After the film deposition the solvent and other organic ingredients have to be removed, which is done by sintering the film in 450 – 500 ^{o}C for half an hour minimum. In this treatment the individual TiO_2 nanoparticles also "neck" together and adhere more tightly to the substrate surface which decreases the interparticle resistance, thus facilitating efficient electron diffusion in the film, and the resistance for the electron transfer from the TiO_2 network to the substrate. Unfortunately, this sintering treatment, which drastically improves the TiO_2 film quality and also its mechanical stability can not be employed with plastic substrates, due to their low temperature tolerance. One promising technique for low temperature PE film preparation is spraying suspension of TiO_2 nanoparticles in high volatility solvent (e.g. ethanol) on heated substrate and then mechanically compressing the resulting powder layer. Titania pastes suitable for low temperature sintering have also been developed but the problem of inadequate interparticle necking and thus lower cell efficiency, due to slower electron transport in the film and thus higher recombination probability, still remains with these materials too.

Dye sensitization of the PE is done simply by soaking the TiO_2 film in the dye solution (anhydrous ethanol being the common solvent, though various nitriles have also been used), the soaking time typically being overnight minimum, though the process can be sped up by heating the solution. The dye is one of the most expensive components of the cell, due to the complex structure and demanding, multistep synthesis of the molecule, but since its amount in the solution is very small, typically of the order 10^{-4} M, its effect on the overall manufacturing costs of the cell remains reasonably low. In addition to the ruthenium organometallic complexes mentioned already in chapter 2.3, other dyes such

as coumarins, eosins, perylenes and even natural dyes extracted from berries have been employed in the DSC, though the highest efficiencies have still been obtained with the Ru-complexes. As a matter of fact, the molecular structure of the dyes and the electron transfer processes in the dye excitation resemble those of the chlorophyll molecule in green plants, which is why the DSC operating principle has sometimes been called "artificial photosynthesis".

2.4.3 Electrolyte

In addition to the redox couple – like the most commonly used iodide/triiodide – the electrolyte usually contains some "blocking agent" that adsorbs on the PE on those surface sites not occupied by the dye to prevent recombination, i.e. electron leakage from the TiO_2 back to the electrolyte. 4-*tert*-butylpyridine, guanidinium thiocyanate and 4-guanidinobutyric acid are some molecules used in this purpose [2, 29]. Due to suppressed recombination, the cell open circuit voltage increases. The requirements for the electrolyte solvent are its ability to dissolve the other ingredients and preferably low volatility combined with high viscosity to facilitate fast ionic diffusion between the electrodes. Typical solvents used in the DSC electrolyte are various nitriles (aceto-, methoxypropio-, valero-, butyro-), carbonates (ethyl-, propyl-) and their mixtures. Liquid electrolyte can also be gelatinized, for example with certain polymers (e.g. polyvinylidenefluoride-hexafluoropropylene, PVDF-HFP) or silica nanoparticles [30]. While this does not remove the problem of the cell "drying" in case of structural damage to the substrates, it does prevent electrolyte leakage. Obviously, the liquid electrolyte is the weak link considering the cells' long-term stability which is why solid hole conductors such as copper iodide (CuI), copper thiocyanate (CuSCN), copper bromide (CuBr) complexes, 2,2′7,7′-tetrakis-(N,N-di-p-methoxyphenyl-amine)-9,9′-spirobifluorene (spiro-MeOTAD), and the conducting polymer poly(3,4-ethylenedioxythiophene) (PEDOT) have also been studied as its replacement [31-41]. Either the cell efficiency or its stability have not been satisfactory with these – one reason being the solid material's poor penetration into the pores of the TiO_2 layer – which is why iodine-based liquid electrolyte is still the most often used alternative in the DSC. An example of a typical electrolyte composition is 0.5 M lithium iodide (LiI), 0.05 M iodine (I_2), and 0.5 M 4-*tert*-butylpyridine in 3-methoxypropionitrile (triiodide ions are generated in a reaction of molecular iodine with the iodide ions). The amount of iodine may vary according to the electrolyte layer thickness – in cases where the light enters the cell from the counter electrode (CE) side, through the CE and electrolyte (e.g. if the PE is deposited on opaque metal sheet), the shadowing effect of the dark red triiodide ions in the electrolyte reduces the amount of photons reaching the PE (iodide ions, on the other hand, are transparent). When the order of the maximum current the cell should be able to generate is known, the triiodide concentration and electrolyte layer thickness can be minimized using the definition for the diffusion-limited current density [42]

$$i_{\lim} = \frac{2nFD_{I3-}c_{I3-}}{l}, \tag{6}$$

where n is the number of electrons transferred in the redox reaction, F the Faraday constant, D_{I3-} the triiodide diffusion coefficient, c_{I3-} the triiodide concentration, and l the distance between the electrodes.

There is also an interesting, new group of DSC electrolytes in which so-called ionic liquids, or room temperature molten salts are utilized [43-45]. Ionic liquids are fluids with no vapor pressure at all which eliminates the problem of electrolyte drying in case of fractures on the substrate. Typically, ionic liquids are salts of iodine with a large, often imidazole-based cation, for example 1-methyl-3-propylimidazolium iodide (PMII) or 1,2-dimethylimidazolium iodide (DMPII). Thus, ionic liquid works as a source of iodide ions and also as a solvent, due to its fluidic nature. The problem of these electrolytes is, however, the high viscosity of many ionic liquids, which slows down the ionic diffusion and tends to keep cell efficiencies down. Some ionic liquids are also hygroscopic which means that special conditions, e.g. dry air or nitrogen atmosphere is needed for cell preparation and storage of materials.

2.4.4 Counter electrode

For DSCs deposited on glass, thermally deposited or sputtered platinum is the most widely used CE catalyst. The advantages of Pt are its high catalytic activity towards the iodide/triiodide redox reaction which is why only a few nanometer layer of Pt is required – this keeps the cell manufacturing costs low even if Pt is an expensive element, and because the thin Pt layer is almost transparent, platinized counter electrodes can be employed also in cells which require reverse lighting (i.e. lighting from the CE side). Platinum is also chemically stable in the electrolyte, i.e. no remarkable dissolution over time from the CE have been noticed (in case the CE catalyst dissolves and diffuses to the PE, it may act there as recombination centers, thus decreasing the cell efficiency). In the thermal method, an alcoholic solution of platinum salt (e.g. $PtCl_4$ or H_2PtCl_6) is spread on the substrate and after the solvent evaporation, the substrate is fired in an oven in 385 ^{o}C for ca. 15 minutes. This results in reduction of metallic platinum as tightly adhered nanoscale clusters on the substrate surface [46]. Due to high temperature involved, this method is naturally not suitable for plastic substrates but sputtering, which is a well known and widely applied method for thin film coatings, can be employed for low temperature tolerance substrates as well.

Since platinum is an expensive catalyst, even if the consumption is relatively low, other materials such as nanostructured and/or activated carbon and conducting polymers such as PEDOT or PANI (polyaniline) have been studied as its replacement [18]. The main problem with these materials is that often rather thick layers of them are needed in order to reach high enough catalytic activity. This slows down the cell manufacturing process and, as thick catalyst layers also absorb light, these kind of CEs are not suitable for reverse lighting cells. Carbon materials are also typically deposited from sprayable suspensions (cf. the TiO_2 suspension spraying technique for plastic substrates), and the mechanical integrity of the resulting powder film is achieved with simple compressing. Since in the compressing process no chemical or physical bonds between the powder

particles and the substrate are formed the stability this kind of a film has against mechanical stress is not as good as that of a few nanometer layer of thermally deposited or sputtered platinum.

2.4.5 Cell assembly

The electrodes are typically laminated together on a hot plate, using a thermoplastic ionomer resin film (e.g. Surlyn®, Bynel®) as a sealant and spacer to prevent the cell from short circuiting. So-called glass frit technique can also be used but since it requires high temperatures, it is suitable only for glass substrate cells [47]. After this, the electrolyte is inserted into the cell through special filling channels drilled on either one of the substrates or cut to the spacer film on the sides of the cell. The filling channels are sealed and the external current collectors applied, after which the cells are ready for encapsulation. Figure 11 presents an example of a manufacturing process of a flexible and low temperature spray-deposited DSC.

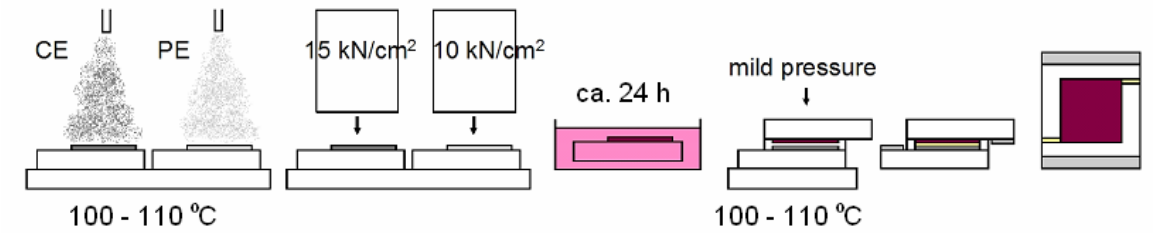

Figure 11. A low-temperature preparation process for flexible DSCs.

2.5 State of the art in DSC on different substrates

The highest reported DSC efficiencies at the moment are around 10-13 % with all-glass substrates, which is well comparable for example to amorphous silicon solar cells [48]. The highest flexible DSC efficiency is close to that also: 8.6 % with a stainless steel PE cell [27] (Pt-sputtered ITO-PEN as the CE). With stainless steel CE, even 9.15 % was achieved, using high active surface area carbon black as a catalyst, though in this case the PE was deposited on glass, so the cell was not completely flexible [18]. Titanium has also been successfully used as the PE substrate, giving efficiency of 7.2 % (flexible cell with platinized ITO-PEN as the CE) [24]. With all-plastic substrates, a promising 7.4 % has been achieved utilizing, in the deposition of the TiO_2 film, the suspension spraying and compressing technique mentioned earlier [49]. In [49], also the TiO_2 nanoparticles were self-synthesized and very high compressing force was noticed to be the key factor in improving the compressed PE cell efficiency. Typically, the plastic PE cell efficiencies have been on the range 5-6 %, using methods such as hydrothermal crystallization [50-52], chemical vapor deposition of Ti alkoxides [53-55] combined with microwave or UV treatment [53-56] or laser sintering [57] as a replacement of the high temperature post-treatment of the TiO_2 film.

It must be noted here, however, that cell efficiencies are not automatically comparable – for example, different electrolyte solvent, different manufacturer of the TiO_2 paste/particles or different substrate pre-treatment methods may directly affect the efficiency. In top efficiency cells, also several "efficiency-boosting" means such as anti-reflectance coatings, large, scattering TiO_2 particles in the PE film and additional recombination blocking layers between the substrate and the TiO_2 film may have been utilized. In addition to this, the top efficiencies are typically obtained with very small cells (active area < 1 cm^2). When the active area size increases the substrate sheet resistance is bound to cause remarkable ohmic losses unless metal substrates or additional current collector structures embedded to the substrate material are used. When the cells are further combined to modules, additional resistance occurs also in the wirings between the individual cells.

All in all, high efficiencies alone are not enough to make the DSC appealing to consumers and investors – long-term stability is still a relatively little studied issue, especially in the case of metal- and plastic-based cells. Stability improvement has been achieved with development of new dyes, for example with hydrophobic Z-907 less than 10 % drop in efficiency in 1000 hours 80 ^oC heating test was measured [58]. Also, in simple light-soaking tests even longer stability times have been reported, like 12 000 hours at one Sun [59] and 8000 hours at 2.5 Sun [60]. However, factors like the chemical stability of the electrolyte, the chemical stability of the metal substrates, the penetration of water and oxygen into the cell (especially with plastic substrates) and the effect of varying environmental conditions during the cell operation are still topics that need more thorough research to make this technology fully competitive against the traditional crystalline silicon PV devices. The special treatments that may be needed to increase the DSC efficiency to maximum also cause additional, possibly expensive steps to the manufacturing process and thus may increase the cell price too much.

Commercialization-wise, DSC-based PV devices are not yet generally available in the same way silicon and some types of thin film panels are. There exist several companies though which are already very close: For example, Australian Dyesol, Inc. is the current leader in industrial-scale DSC material development and marketing [61]. Their large scale cooperation with the leading steel industries also indicates that metal-based DSC looks like a promising route to bring this technology out of laboratory and into public use. Other companies that already have automated, high throughput DSC production are G24 Innovations, Inc. in Great Britain [62] and Konarka, Inc. in the USA [63]. Common to all these companies is roll-to-roll manufacturing of the DSC on flexible, plastic or metal substrates, products including for example mobile phone chargers and "electric fabric" (Figure 12). Dyesol also manufactures more conventional, glass-based BIPV (building integrated photovoltaics) tiles and panels (Figure 13).

Figure 12. Examples of flexible DSC products. Pictures © G24 Innovations.

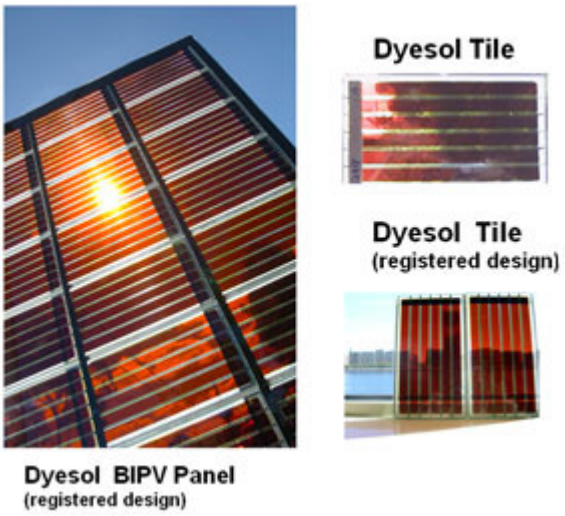

Figure 13. BIPV DSC panels and tiles. Pictures © Dyesol.

3 Research methods

Information about a solar cell performance can be obtained with several experimental methods, including spectroscopical techniques and electron microscopy for materials characterization. However, since the central results included in this thesis were from current-voltage curve and electrochemical impedance spectroscopy measurements, only these two methods are described here more detailedly.

3.1 Current-voltage curve measurements

Current-voltage curve measurements are the most central way to characterize the PV device performance. In these measurements, the lighted cell is put under a reverse bias voltage scan and the generated photocurrent recorded (Figure 14). At the point where the external bias voltage is zero, there is no opposing force to the current flow from the cell and the maximum current the cell is able to generate, the short circuit current I_{sc}, can be measured. Accordingly, at the point where the external voltage equals the maximum voltage of the cell, the open circuit voltage V_{oc}, no current flows. In practice, and to make the results independent of the cell size, current density, expressed in A/cm^2, is used instead of plain current.

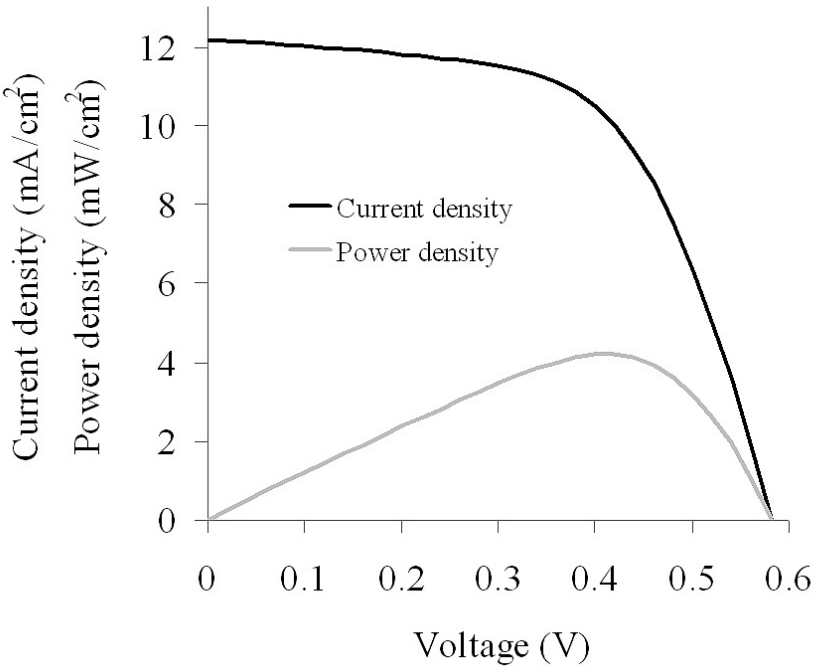

Figure 14. An example of an *IV*-curve and a power curve of a DSC.

From the power curve the maximum power point can be detected and from the current and voltage at this point, I_{mpp} and V_{mpp}, along with I_{sc} and V_{oc}, the fill factor (*FF*) of the cell can be calculated from the equation

$$FF = \frac{V_{mpp} \cdot I_{mpp}}{V_{oc} \cdot I_{sc}}. \tag{7}$$

Fill factor measures the "squareness" of the curve. For example, resistive losses in the cell show directly from the shape of the *IV*-curve, making it "flatter" and decreasing the fill factor. The cell efficiency (η) can be calculated using the fill factor, or directly from the I_{mpp} and V_{mpp} using the equation

$$\eta = \frac{V_{oc} \cdot I_{sc} \cdot FF}{P_{in} \cdot A} = \frac{V_{mpp} \cdot I_{mpp}}{P_{in} \cdot A}, \tag{8}$$

where P_{in} is the power of incident light on the cell and *A* is the photoactive area of the cell, i.e. in the case of the DSC, the area of the dye-sensitized TiO_2 film.

In practice, the cells are measured under artificial lighting in a solar simulator. To ensure that the measurement results are comparable even if the used lighting is different, so-called standard measurement conditions are defined. They are: 25 ^{o}C temperature, 1000 W/m^2 power of incident light, and AM 1.5 G solar spectrum. Temperature and power of incident light can be adjusted with technical means, but to adjust the measured photocurrent to correspond to that obtained with the AM 1.5 G standard spectrum, so-called spectral mismatch factor *M* for the used simulator has to be determined [64]. It can be calculated using a standardized reference cell (for example a monocrystalline silicon cell characterized in an officially, internationally recognized standardizing laboratory) with the formula

$$M = \frac{I_{test,sim}}{I_{test,std}} \cdot \frac{I_{ref,std}}{I_{ref,sim}}, \tag{9}$$

where $I_{test,std}$ is the current of the measured cell under the standard spectrum, $I_{ref,std}$ the current of the reference cell under the standard spectrum, i.e. the value which is known from the standardizing laboratory, $I_{ref,sim}$ the current of the reference cell in the simulator, and $I_{test,sim}$ the current of the measured cell in the simulator, after which the corrected photocurrent for the measured cell is obtained as

$$I_{test,std} = \frac{I_{test,sim}}{M}. \tag{10}$$

The mismatch factor is obviously valid for only one type of lamps that are used in certain solar simulator and in certain measurement geometry.

3.2 Electrochemical impedance spectroscopy

IV-curve measurements give only quite superficial information about the cell operation – for instance, they do not directly tell the physical reasons why a cell works efficiently or not. Electrochemical impedance spectroscopy (EIS) is a valuable tool to probe deeper the charge transfer phenomena and electrochemical processes in the cell components and interfaces. In EIS, a small amplitude (typically mV scale) AC voltage signal which frequency is varied over a certain range is set over the cell and the resulting AC current signal recorded. Since different charge transfer phenomena show at different frequencies, depending on their time scale, the impedance responses of the cell components can be individually distinguished from the spectra. During the measurement, the cell can be externally polarized to some target voltage or it can be set under lighting and measured at the resulting open circuit voltage. The cell impedance is then obtained as a function of the (angular) frequency ω of the AC voltage signal from the definition

$$Z(\omega) = \frac{V_{AC}(\omega)}{I_{AC}(\omega)}. \tag{11}$$

The impedance data is typically presented either as a Bode or a Nyquist plot. In the Bode plot, the real and imaginary parts of the impedance are shown as a function of frequency and in the Nyquist plot, the x-axis represents the real impedance *Z'* and the y-axis the imaginary impedance *Z"* in the complex plane. Figure 15 presents an example of a Bode plot and Figures 17, 19 and 22 examples of Nyquist plots.

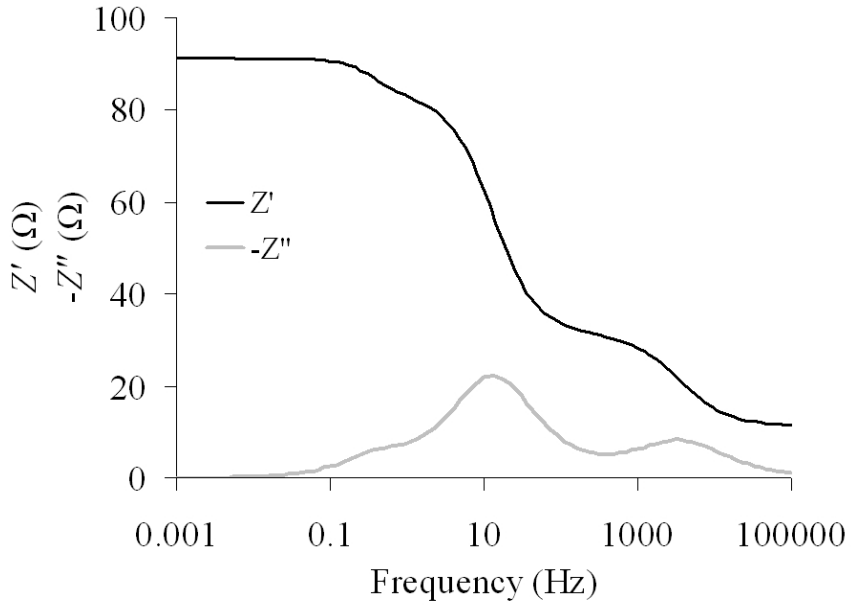

Figure 15. A Bode plot of a simulated impedance spectrum of a DSC. Frequency span in the simulation 1 mHz – 100 kHz.

Interpretation of the impedance spectra is done by utilizing so-called equivalent circuits. In them, the cell components and interfaces are presented as electrical components such as resistors and capacitors. By fitting the measured impedance spectrum to the equivalent circuit, numerical values for the parameters such as resistances in the cell components, capacitances on the electrode surfaces, and diffusion impedance in the electrolyte can be obtained.

The type of an equivalent circuit used depends on the cell type. The most simple, symmetrical counter electrode – counter electrode cell can be modeled as an *RC*-circuit in series with a resistor, as presented in Figure 16. Also, the Warburg element W_s describing the impedance for the ionic (Nernstian) diffusion in the electrolyte, Z_d, is added. Figure 17 presents a Nyquist plot of a simulated spectrum based on the equivalent circuit in Figure 16.

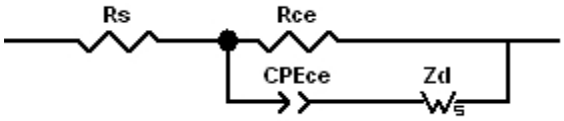

Figure 16. A symmetrical CE – CE cell equivalent circuit.

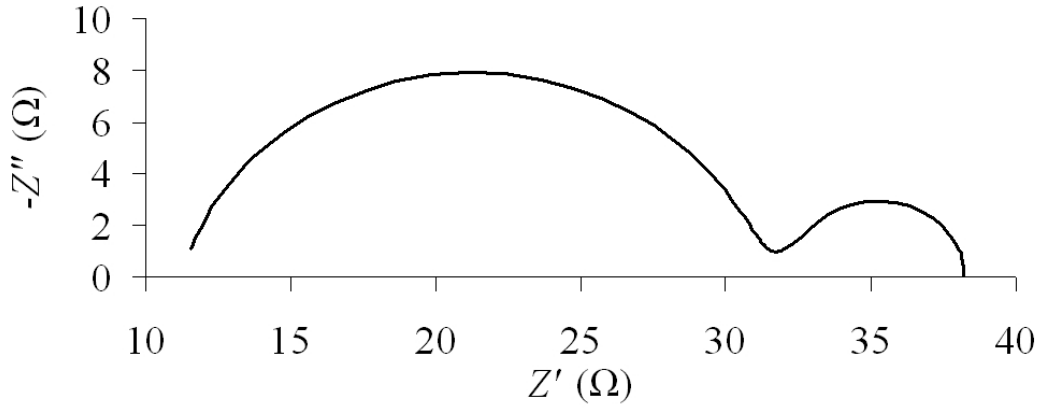

Figure 17. A Nyquist plot for a simulated impedance spectrum for a symmetrical CE – CE cell. Frequency span in the simulations 1 mHz – 100 kHz.

In Figure 16, the single resistor describes the total ohmic losses in the cell, the cell series resistance R_s, whereas the *RC*-circuit the interface between the electrode surface and electrolyte. Charge transfer resistance R_{ce} measures the activity of the CE catalyst: The smaller the R_{ce}, more effectively the triiodide reduction reaction proceeds. Electrode capacitance, on the other hand, originates from the charge accumulation: Accumulation and orientation of oppositely charged ions from the electrolyte results in formation of a Helmholtz dipole layer on the electrode surface which works as a miniature capacitor. In practice, pure capacitance is a valid model only for completely "smooth", homogenous

electrode surface. This is why, in the case of the DSC where surface inhomogenities arise simply from the fact that the catalyte is not evenly spread or the surface is porous, so-called constant phase element *CPE* is used in the equivalent circuits instead of a plain capacitance. The capacitance of a *CPE* is defined with the equation

$$Z_{CPE} = \frac{1}{B_0}(i \cdot \omega)^{-\beta}, \tag{12}$$

where the pre-factor B_0 has units of capacitance and the exponent β is related to the "flatness" of the semicircle [65]. The more the exponent deviates from one, the farther the electrode surface is from an ideal capacitor which shows as "flattening" of the semicircle.

In Figure 17, the larger semicircle on the left, high frequency end of the plot arises from the R_{ce} – CPE_{ce} parallel combination whereas the series resistance can be obtained as the distance between origin and the start of the R_{ce} – CPE_{ce} semicircle. The diffusion impedance shows as the smaller semicircle on the right, low frequency end of the plot.

Figure 18 presents a "simplified" equivalent circuit for a complete DSC and Figure 19 again a simulated spectrum according to Figure 18. Here, two *RC*-circuits are used, another for the photo- and another for the counter electrode. This kind of a simplified circuit can be used in cases where, in the photoelectrode impedance response, only the recombination resistance part is shown in the spectrum. In reality, the PE total resistance R_{pe} is a combination of the electron transport resistance in the TiO_2 film, R_{tr}, and the charge transfer resistance for the electron recombination reaction across the TiO_2 – electrolyte interface, R_{rec}, but the former component typically shows only when the electron transport in the TiO_2 film is somehow "hindered", i.e. on small external polarization voltages when the film conductivity is low due to small amount of electrons in it or in cases where the resistance for the electron transport is high because of poor film quality. So, in the equivalent circuit in Figure 18, R_{pe} equals R_{rec}.

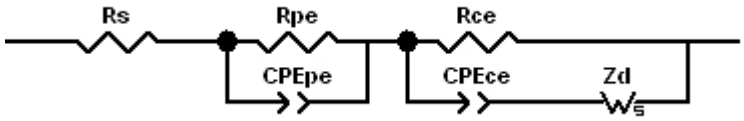

Figure 18. A simplified complete DSC equivalent circuit.

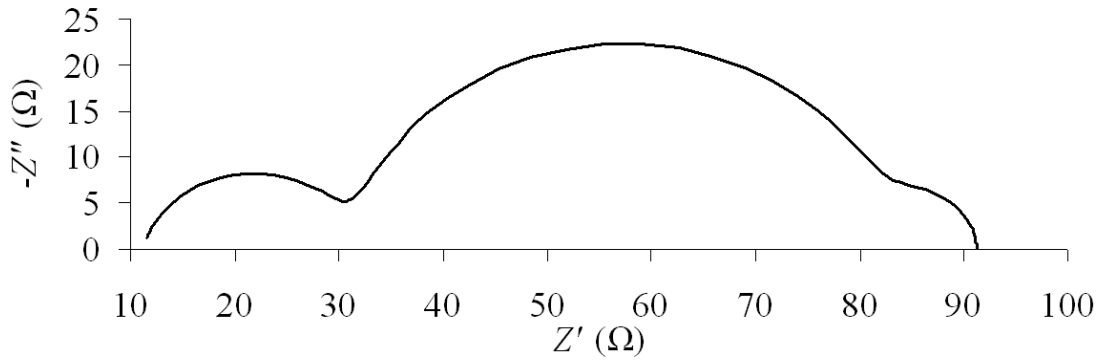

Figure 19. A Nyquist plot for a simulated spectrum for a complete DSC, according to the equivalent circuit in Figure 17. Frequency span in the simulations 1 mHz – 100 kHz.

In Figure 19, the series resistance is again the distance from the origin to the starting point of the first semicircle, the *RC*-circuit describing the CE generates the first semicircle from the left, the large semicircle in the middle originates from the parallel combination R_{pe} – CPE_{pe} at the photoelectrode, and the small semicircle on the right, partially overlapped by the PE semicircle, describes the diffusion impedance. Charge transfer resistance both on the CE surface and for the recombination reaction at the PE can be obtained also visually from the Nyquist plots as the diameter of the corresponding semicircles. Additionally, in the case of a symmetrical CE – CE cell, the result has to be divided by two, since the impedance responses of two identical electrodes overlap. To obtain the photoelectrode surface capacitance from the *CPE* impedance, the definition for the electron lifetime τ_e in the TiO_2 film can be used [66].

$$\tau_e = (R_{rec} \cdot B_0)^{1/\beta}, \tag{13}$$

where the pre-factor B_0 and the exponent β are the same as in equation 12. Since τ_e can also be interpreted as the time constant of the *RC*-circuit describing the PE, i. e.

$$\tau_e = R_{rec} \cdot C_{pe}, \tag{14}$$

combining the equations 13 and 14 enables calculation of the photoelectrode capacitance (equation for the counter electrode capacitance is analogous)

$$C_{pe} = \frac{(R_{rec} \cdot B_0)^{1/\beta}}{R_{rec}}. \tag{15}$$

To make the results independent of the electrode size, the charge transfer resistances are typically expressed as Ωcm^2 instead of only ohms, and the capacitances as F/cm^2, instead of only faradays. This way, analogously to the *IV*-curves where the photocurrent is

expressed as A/cm^2, the numerical values obtained are characteristic to the material, not just a single cell.

If the electron transport resistance shows in the PE impedance response, it manifests itself as a short, straight line of angle 45^o between the CE and PE semicircles. In cases where the transport resistance is so high that the electron diffusion length in the TiO_2 film remains shorter than the film thickness (i.e. high recombination probability and only a small amount of photogenerated electrons can be collected), the whole PE semicircle takes the shape characteristic to the Gerischer impedance and it becomes impossible to define absolute values for either of the PE resistance components [67]. Figure 22 presents examples of the DSC impedance spectra, where the transport resistance and Gerischer impedance can be seen. In this kind of cases, where the PE impedance response is not a "clean" semicircle, fitting the so-called transmission line element [67-69] to the PE spectrum gives a more accurate result. In the transmission line model the transport resistance in the TiO_2 film, as well as the charge transfer resistance-capacitance combination on the TiO_2-electrolyte interface are modeled as a distribution of infinitesimally small resistance and capacitance elements instead of one uniform value describing the whole film or interface. Figure 20 presents a schematic of a pore in the TiO_2 film, modeled with the transmission line and Figure 21 a detailed, complete DSC equivalent circuit where also the interfaces TiO_2-substrate (R_{co} – CPE_{co}) and electrolyte-substrate (R_{su} – CPE_{su}) are included. In practice, however, the impedance responses originating from these interfaces occur on such frequencies that they get overlapped by the more prominent CE and PE impedance arcs.

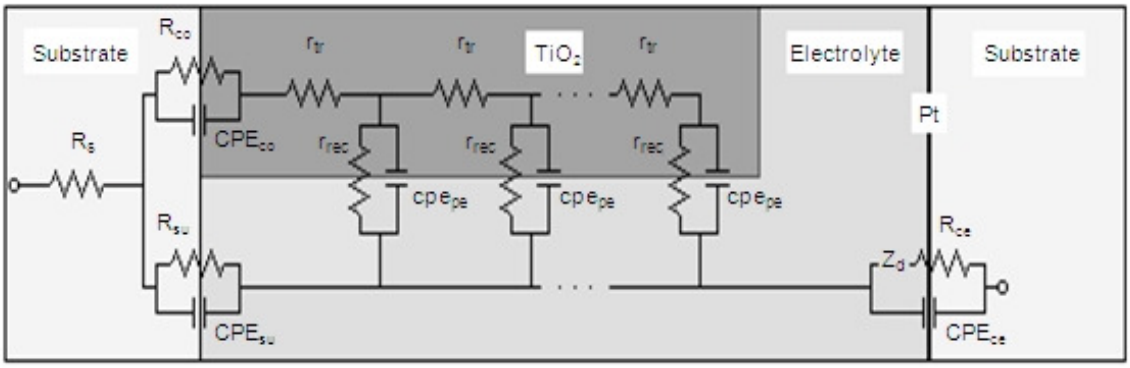

Figure 20. A schematic of a pore in the TiO_2 film, described with the transmission line model. r_{tr}, r_{rec} and cpe_{pe} are the distributed transport resistance, recombination resistance and photoelectrode capacitance elements, respectively. Modified from the picture presented in [67, 68].

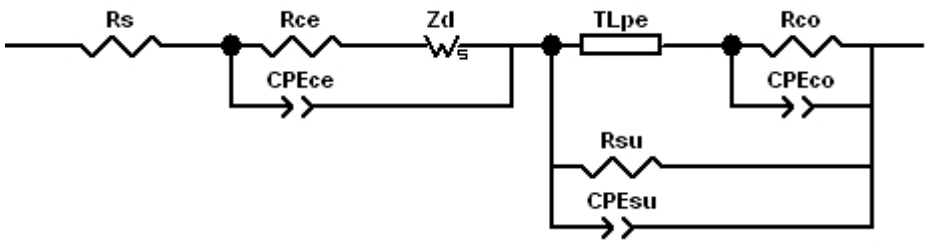

Figure 21. A detailed DSC equivalent circuit, including the TiO_2-substrate and electrolyte-substrate interfaces and a transmission line element TL_{pe} to describe the photoelectrode.

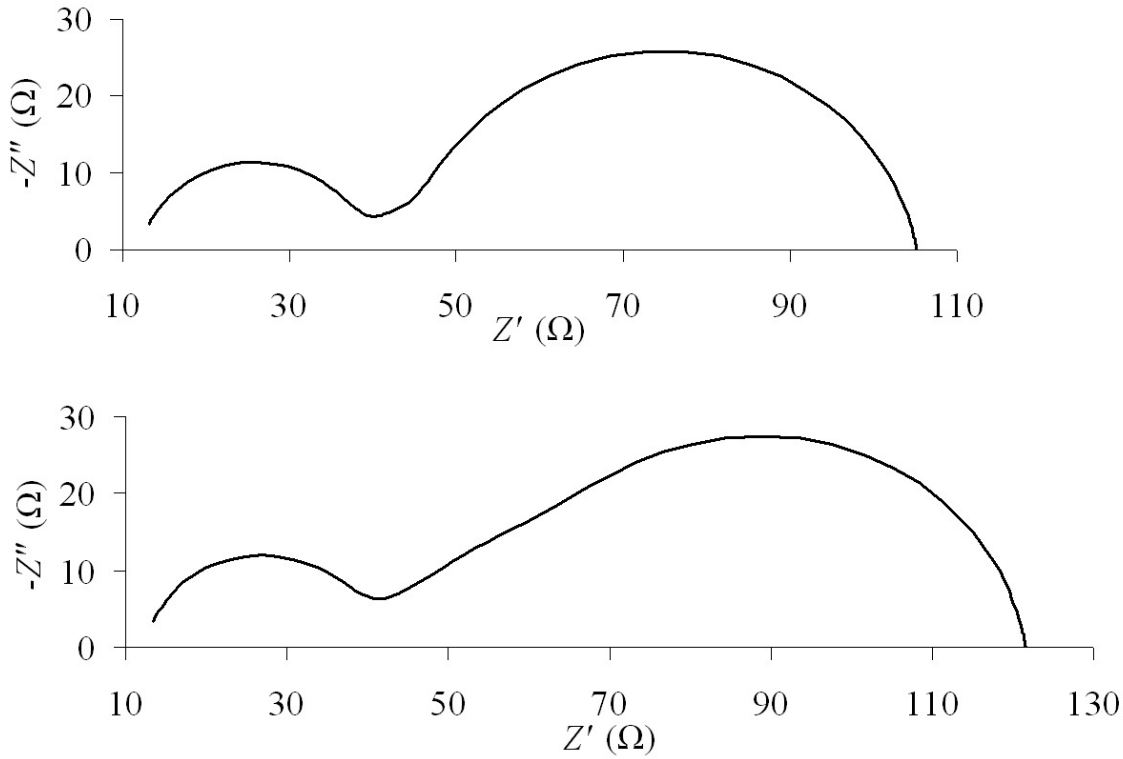

Figure 22. Nyquist plots for simulated examples of a spectrum where the transport resistance "line" shows between the CE and PE impedance semicircles (top) and a spectrum with a Gerischer-shaped PE impedance response (below). Frequency span in the simulations 1 mHz – 100 kHz. Diffusion impedance not shown in these spectra.

4 Experimental work

4.1 DSC materials and preparation

In the course of this thesis, the DSC preparation was investigated on ITO-PET and ITO-PEN plastics, stainless steel, carbon steel and copper sheets and as a reference, FTO-coated conducting glass substrates. Also, DSCs of cylindrical geometry were deposited on glass and PMMA (polymethylmethacrylate) plastic optical fibers. ITO-PET (sheet resistance 60 Ω/□ and thickness 190 µm) was provided by Bekaert, Inc., ITO-PEN (sheet resistance 15 Ω/□) by Peccell, Inc., stainless steel (type 1.4301, thickness 0.8 – 1.25 mm) by Outokumpu, Inc., carbon steels (both Zn-coated and plain, thickness 1 mm) by Ruukki, Inc. and copper (thickness 0.63 mm) by Luvata, Inc. Fluorine-doped tin oxide (FTO) glass (Pilkington TEC-8 with sheet resistance 8 Ω/□ and thickness 3 mm and Pilkington TEC-15 with sheet resistance 15 Ω/□ and thickness 2.5 mm) was supplied by Hartford Glass Company, Inc. Optical fibers were provided by Baltronic, Inc. (PMMA plastic) and Photonium, Inc. (glass).

The pre-treatment of all substrates was similar: First, they were washed with warm water and mild detergent, rinsed and let dry, after which the cleaning was finished in an ultrasonic bath first three minutes in ethanol and then three minutes in acetone. After this, the substrates were dried with pressurized air. The size of the substrates varied from the 16 mm x 20 mm for the small, laboratory-scaled test cells to 6 cm x 6 cm for the "mini-modules" with which cell upscaling issues were studied.

Photoelectrodes were deposited both with doctor-blading method using commercial TiO_2 paste (Sustainable Technologies International) and with spraying from self-made suspension of 20 wt% TiO_2 nanoparticles (P25 from Degussa) in absolute ethanol. Doctor-blading was tried also with the suspension and since it worked well, this deposition technique was adopted for low temperature photoelectrodes too. Since the commercial paste requires sintering as post-treatment, it was obviously used only on glass and metal substrates. Two or three layers of paste/suspension was spread through a mask cut of regular office tape of 60 µm thickness. Between the layers, the substrates were let to dry on a hot plate (100 – 110 ^{o}C) and in the case of the suspension, room temperature compression in a hydraulic press (pressure 125 – 250 kg/cm^2) was applied to improve the particle adhesion on the substrate. As the final treatment, the glass and metal photoelectrodes were sintered in 450 – 500 ^{o}C for half an hour and for the plastic photoelectrodes, one final compression in the press was applied. The final thickness of the TiO_2 films was 10 – 15 µm. On the glass optical fibers the TiO_2 was applied by dipping the fibers into diluted TiO_2 paste, after which the fibers were sintered analogously to the glass substrates. On the plastic optical fibers, since compressing cylindrical samples would have been difficult, the TiO_2 layer (50 nm) was coated with atomic layer deposition (ALD) method. Since the fiber substrates were not conductive as such, a 130 nm of ZnO:Al was applied with the ALD prior to the TiO_2 deposition. The dye-sensitization of the photoelectrodes was done by soaking them in 0.32 mM anhydrous ethanol solution of the N-719 dye (cis-bis(isothiocyanato)bis(2,2'-bipyridyl-

4,4'-dicarboxylato)-ruthenium(II) bis-tetrabutylammonium, Solaronix SA) for one day minimum, after which the electrodes were rinsed and stored in absolute ethanol.
Platinized counter electrodes were prepared on glass, plastic and stainless steel substrates, the glass ones being the reference against which the performance of the other types of CEs were compared. On glass and steel, platinization was done with the standard thermal method described in Chapter 2.4.4. Plastic substrates were platinized by sputtering. Since Pt is an expensive CE catalyst, activated carbon and graphite based powder materials were investigated as its replacement. Also, a platinized Sb:SnO_2 powder was studied since it is, like the carbon powders, possible to be applied without the high temperature post-treatment and could thus be suitable also on plastic substrates. The compositions of the carbon-based and platinized Sb:SnO_2 powder materials were based on the literature, and a modification of the activated carbon and graphite powder was successfully applied also on the cylindrical DSCs on optical fibers. On planar substrates, the carbon and Sb:SnO_2 powder materials were deposited with the spraying method from ethanol-based suspensions, analogously to the TiO_2 suspensions. The mechanical integrity of the film and its adherence to the substrate were achieved with room temperature compressing, again analogously to the TiO_2 powder photoelectrodes. The compression pressure for the CEs was 1000 – 1500 kg/cm^2.

The standard iodine electrolyte described in Chapter 2.4.3 was used in all cells prepared for this study, the only variation being the iodine content which was optimized for the electrolyte layer thickness. In some cases, the electrolyte was also gelatinized in order to improve the mechanical strength of the electrolyte layer or its applicability, like in the case of the optical fiber DSCs where all cell layers had to be deposited by the dipping method. Before the electrolyte filling, the electrodes were sandwiched together on a hot plate in 100 – 110 ^{o}C using a 25 µm or 45 µm thick Surlyn® film as a spacer and sealant. The electrolyte iodine content corresponding to these two spacer thicknesses was either 0.03 M or 0.05 M, respectively.

4.2 Cell characterization – measurements and equipment

The *IV*-curves were measured with a custom-made solar simulator equipped with ten 150 W halogen lamps as the irradiation source and a temperature-controlled measurement plate on which the cell temperature could be adjusted to 25 ^{o}C. The irradiation intensity was set to the standard 1000 W/m^2 with a calibrated monocrystalline silicon reference cell equipped with a spectral filter to mimic a typical DSC response. The mismatch factor of the simulator was used to make the *IV*-curves correspond to the standard AM 1.5 G solar spectrum. The optical fiber DSCs were measured either with side lighting in the solar simulator or by coupling the light into the DSC fiber with a pigtail fiber.

The EIS data was recorded with Zahner Elektrik's IM6 impedance measurement unit operated with Thales software and the equivalent circuit fits were done with the ZView software from Scribner, Inc. The cell lighting for the EIS measurements was provided with a red LED of wavelength 640 nm and with the irradiation of ca. 8 % of one sun intensity. To protect the cells from stray light, they and the LED were put inside a black

box for the measurements. For the temperature-ramped EIS measurements described in Publication IV, the cells were put on a Pt-1000 temperature sensor controlled hot plate.

5 Results and discussion

5.1 Low temperature depositable counter electrodes for plastic substrates (Publication I)

Whilst platinum still remains the most widely used and efficient CE catalyst in the DSC and can be applied, in addition to the high temperature thermal method [46], also with sputtering which is a suitable technique also for low temperature tolerance substrates such as plastics, it is an expensive and, as a rare noble metal, not so abundant catalyst material. Sputtering is also a technique which is difficult to integrate to continuous throughput roll-to-roll type manufacturing process, it requires vacuum and wastes quite much of the sputtered material, considering the sputtered layer forms not only on the substrate but on the walls of the sputtering chamber as well. This is why, in order to realize a fully flexible, cost-efficient and industrial-scale producable DSC, it is important to find catalysts which are low price, easily available and depositable with industrially upscaleable methods.

Several carbon-based materials have been presented in the literature, for example activated carbons with different surface areas (carboxymethylcellulose as a binder) [70], a mixture of carbon black and graphite (TiO_2 nanoparticles as the binder) [71], and single-wall carbon nanotubes [18] which, in addition to being an efficient catalyst for the triiodide reduction reaction, have also low sheet resistance which could justify their use not only as the catalyst but a replacement for the TCO coating of the substrate at the same time. This is an interesting approach because the TCO coatings are expensive and, if the coating and the catalyst could be deposited at the same manufacturing step, it would also reduce the overall process time and costs. Carbon blacks have also been mixed into composites with polymers [18] or used to improve the contact between the CE and the solid-state DSC electrolyte [72]. The low price and easy availability of the activated carbons and carbon blacks stems from their use in large production volumes in printing, paint and pigment industries. Their catalytic efficiency is based on the small, nanoscale particle size which increases the active surface area, yielding nanoporous electrodes not quite unlike the nanocrystalline TiO_2 on the photoelectrode side, whereas the function of the graphite powder is to reduce the lateral resistance in the electrode film. However, relatively thick layers (ten to several tens of µm) of the carbon-based materials are needed in order to reach large enough active surface areas. This makes the electrode films opaque (not suitable for cells where the lighting comes from the CE side, due to opaque PE substrate such as metal sheets) and risks flaking of the electrode material in case the cell is subject to bending. In addition to carbon materials, platinized $Sb:SnO_2$ nanoparticle powder has also been successfully employed as the CE catalyst in the literature [71].

In Publication I, the carbon black/graphite/TiO_2 powder and platinized Sb:SnO_2 powder deposited on ITO-PET plastics were compared against thermally platinized FTO glasses as DSC counter electrodes. To investigate the repeatability of the spray deposition and room temperature compression method, large series (up to 200) of electrodes were prepared and electrochemical impedance spectroscopy was employed as their characterization method.

The carbon powder suspension for the spray deposition was prepared by grinding the ingredients in a mortar in small amount of ethanol, after which more ethanol was added in order to make the suspension fluid enough for spraying. Platinization of the Sb:SnO_2 nanoparticles was realized by grinding the particles in a solution of Pt salt ($PtCl_4$ in isopropanol – the same solution used for the thermal platinization method) and firing the resulting mixture in an oven in 385 ^oC for 10-15 minutes to achieve platinum's reduction from the solution and adherence to the Sb:SnO_2 particles. After this, the resulting powder was crushed and mixed with ethanol to a sprayable suspension as well. Spraying itself was performed with an airbrush on heated substrates (ca. 100 ^oC) to ensure rapid evaporation of the solvent and formation of even films, after which the films were compressed in a hydraulic press in room temperature with pressures up to 1000 – 1500 kg/cm^2. For the impedance measurements, symmetrical CE-CE cells were prepared according to Figure 23.

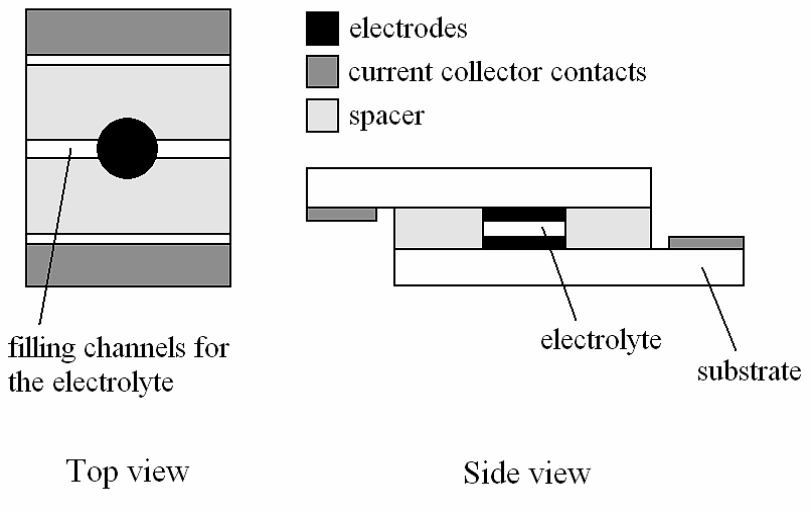

Figure 23. A schematic of a symmetrical CE-CE cell [73].

The benefit of symmetrical CE-CE cells is that no impedance response originating from the PE needs to be taken into account in the data analysis, i.e. the spectra are simpler, consisting (ideally) only of one semicircle describing the charge transfer resistance – capacitance parallel combination on the CE-electrolyte interface. Even the diffusion impedance in the electrode could be neglected in these measurements, due to the porous nature of the electrodes. Porosity increases the active surface area and thus the capacitance of the electrode, which means that the porous electrode's impedance appears

at lower frequencies compared to a planar electrode with the same charge transfer resistance. This can be seen from the equation describing the characteristic frequency f^* of an *RC*-circuit

$$f^* = \frac{1}{2\pi RC}. \tag{16}$$

In practice, the diffusion impedance arc got overlapped by the charge transfer impedance arc in these measurements though on the other hand, an additional, parasitic impedance arc was noticed (Figure 24).

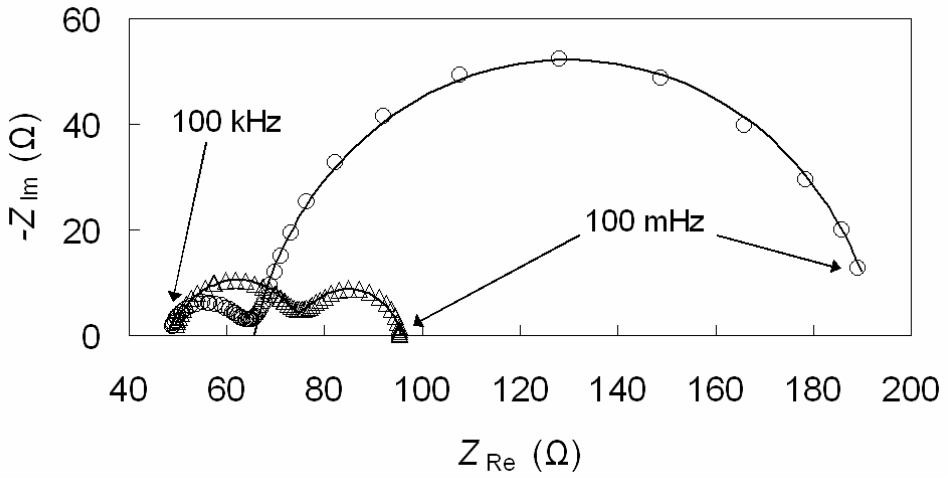

Figure 24. Nyquist plots of typical impedance spectra of porous, compressed carbon powder (Δ) and platinized Sb:SnO2 powder (○) CEs [73].

The parasitic impedance arc on the left, high frequency end of the spectra in Figure 24 was deduced to originate from the bare ITO in contact with the electrolyte in the electrolyte filling channels. At high frequencies, the electrode capacitance hinders the current flow through the electrode-electrolyte interface but an alternative current pathway originates from the parallel coupling of a part of the bare ITO's resistance and the capacitance on the ITO–electrolyte interface. The equivalent circuits in Figure 25 illustrate the situation: In Figure 25 b the cell series resistance R_s is divided in two parts of which the component R_2 describes the part of the ITO's resistance which connects to the ITO capacitance. When this impedance couples with the electrode impedance through the ITO sheet resistance, it gives rise to the additional impedance arc in the spectra. To be exact, the ITO resistance, capacitance and the *RC*-coupling of the electrode charge transfer resistance and capacitance should be modeled with distributed elements, like in the photoelectrode transmission line model described in Chapter 3.2 but the simplified picture in Figure 25 illustrates the situation qualitatively enough. This theoretical explanation for the additional impedance arc was also verified with tests where the bare ITO in the electrolyte filling channels was electrically isolated from the ITO under the electrode. No additional impedance arcs were noticed in these measurements, and the

"standard" CE-CE cell equivalent circuit in Figure 25 a could be used for the data fits for these cells. However, the appearance of the parasitic impedance underlines careful design of the measurement cells and non-uniform, distributed nature of the cell series resistance.

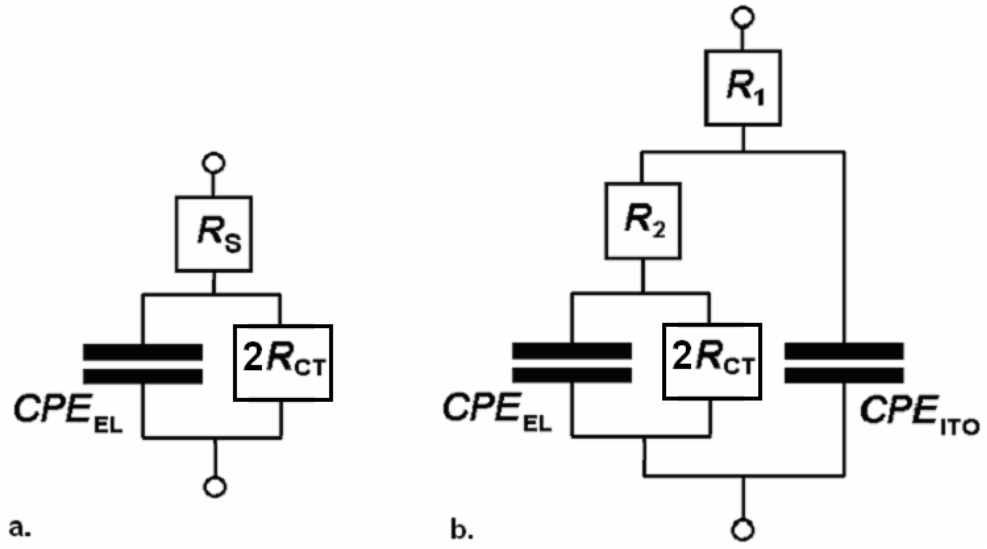

Figure 25. Equivalent circuits used for the data fits in Publication I. a: the "standard" CE-CE cell circuit. b: the circuit for the case where the bare ITO resistance in the electrolyte filling channels couples with the ITO capacitance [73].

The performance of the carbon powder electrodes, characterized with the charge transfer resistance, was very good. With 10-20 µm thick electrodes, charge transfer resistances of 0.5-2 Ωcm^2 were measured, which is even lower than the 4-5 Ωcm^2 obtained with thermally platinized FTO glasses in this study and well comparable to results reported for sputtered platinum electrodes in the literature, 0.8-2.1 Ωcm^2 [42, 74, 75]. For the platinized Sb:SnO_2, the charge transfer resistances were somewhat higher, 8-13 Ωcm^2 for 20-40 µm thick layers, though when proportioned to the Pt loading in these films which corresponds to 1.1-2.3 nm of planar Pt layer, this result is also well comparable to e.g. sputtered Pt films [42, 74, 75]. The repeatability of the spray deposition and compression method was good, yielding large series of even quality electrodes with high speed. The mechanical stability of the Sb:SnO_2 films was better than that of the carbon powder films – it was noticed that when the film thickness exceeded 40 µm, carbon films tended to flake off. Also, long enough grinding of the carbon powder suspension ingredients proved to be crucial for high quality electrodes: Less than 15 minutes grinding yielded electrodes with charge transfer resistances from 70 Ωcm^2 to several hundreds of Ωcm^2 and also poorer adherence to the substrate.

All in all, spray and compression depositable powder materials seemed promising alternatives to Pt in flexible DSCs manufactured with high throughput roll-to-roll methods. Mechanical stability and qualitative evenness of the films was satisfactory for small, laboratory-scale test cells but in order to drastically increase the cell size,

additional stability-improving agents such as binders need to be mixed into the material to improve the interparticle contacts and adherence to the substrate.

5.2 Preliminary tests on industrial sheet metals for DSC substrates (Publication II)

In addition to plastics, metal materials are another group of substrates that could realize both flexible and cost-efficient DSC. The underlying motive in Publication II was to investigate if common industrial sheet metals such as carbon or stainless steels (StS) could be used as the DSC substrates as such. With this approach, the DSC could work as a light-active functional coating on top of the metal sheet realizing for example roofing and façade materials that would produce electricity at the same time. This kind of building materials would save the costs of additional supporting structures of the PV panels, thus facilitating easy installation and implementation of solar electricity and also widen the product variety of metal industries.

Compared to glass and plastics, metals have been studied relatively little as DSC substrates [e.g. 19-27]. In this study, the suitability of several types of Zn-coated and plain carbon steels, stainless steel and copper in this function was preliminarily investigated with soaking and encapsulation tests. In soaking tests, small pieces of the metal materials were immersed in the standard liquid iodine electrolyte described in chapter 2.3.3 and in encapsulation tests, a small amount of the electrolyte was sealed between the metal sheet and glass in order to mimic more closely the situation in the real cell. The soaking test samples were stored in outdoor light, room light or dark to see if lighting conditions had any effect on the behavior of the metals in the electrolyte, and after several weeks the metal ion concentrations in the electrolyte were measured with atomic absorption spectrometry.

Of the studied metal materials, only stainless steel showed sufficient stability in the electrolyte to be employed as DSC substrate as such. The main problem concerning metal substrates in the case of the DSC is the iodine electrolyte since, according to reaction

$$M + I_3^- \rightarrow M^{2+} + 3I^-, \tag{17}$$

where M = arbitrary metal atom/ion, triiodide ions are corrosive towards most metals. Since the triiodide ions give to the electrolyte its distinctive dark reddish color but the iodide ions are colorless, the reaction shown in (17) turned out to be also an easy visual way to inspect the stability of metals in the presence of the electrolyte. For example, in the encapsulation tests, the dark reddish color disappeared in only a few seconds when the electrolyte was encapsulated against a copper sheet. The Zn-coated carbon steel samples corroded relatively fast also, in only a few hours. Oxidizing the Zn-coatings in an oven in 600 ^{o}C was tried in order to make the coatings more resistive towards corrosion (metal oxides are usually more stable than pure metals and ZnO electrodes have been employed in the DSC [e.g. 76]) but not even this treatment could prolong the stability to more than one day maximum. Compact, spray-pyrolyzed TiO_2 and ITO thin

films were also investigated as corrosion protection coatings but obviously the films had so much microscale porosity that they did not noticeably improve the metal samples' stability. In the soaking tests, the electrolyte color started to fade in only a few days in the presence of Zn-coated carbon steels or copper (Figure 26). Surprisingly, plain carbon steel showed somewhat better stability, the complete disappearance of the electrolyte color in the encapsulation tests not occurring until after two months. For stainless steel samples, no visual signs of corrosion or metal ions in the electrolyte could be detected even after 12 months of exposure to the electrolyte.

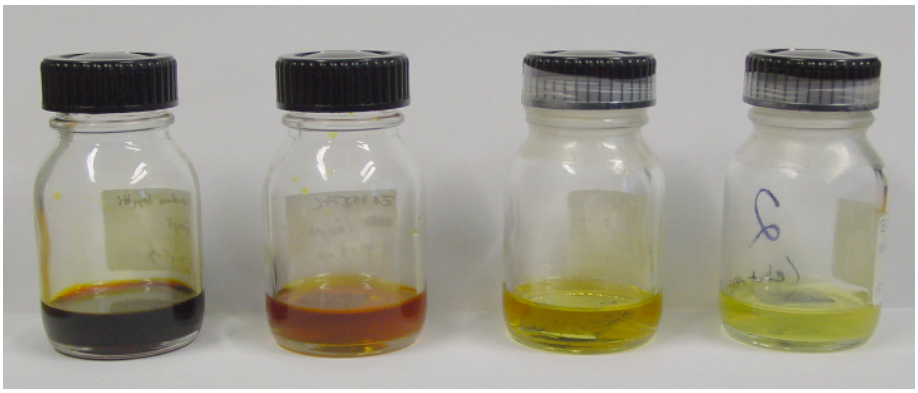

Figure 26. The gradual fading of the electrolyte color in the presence of a corroding metal sample. Left: initial color; right: final color [22].

Based on the soaking and encapsulation tests, stainless steel and carbon steel were chosen for further studies. The metal sheets were employed as counter electrodes and their performance characterized with impedance spectroscopy and with *IV*-curve measurements from complete DSCs.

Plain metal sheets showed no catalytic activity at all, their charge transfer resistances being of the order 10^3 – 10^{13} Ωcm^2, which is why they were platinized with the thermal method analogously to TCO glass substrates. After platinization, charge transfer resistances around 20 Ωcm^2 were achieved, yielding cells with 3.6 % efficiency with a stainless steel CE and glass PE and 3.1 % with a carbon steel CE and glass PE (cf. 4.6 % with an all-glass cell in this study). The series resistances of the cells were only 2 Ω (with glass cells typically around 10 Ω), which is due to the steel substrates' superior conductivity (sheet resistances of metal materials are of the order mΩ/□). In the literature, at the time of this research, 4-5 % efficiencies were obtained with platinized stainless steel and nickel CEs though not all of the results are directly comparable since additional oxide layers were deposited on top of the steel in some of these studies [20, 21, 77]. Other platinization methods than the thermal deposition were also used which may have resulted in different quality, microstructure and morphology of the Pt films.

Despite the promising efficiencies, the fill factors of the stainless steel and carbon steel CE cells were relatively low, ca. 35 %, which indicates high resistive losses somewhere

in the cell, even in spite of the metal substrate's high conductivity. Platinum's poorer adhesion to the metals, compared to TCO glass (the platinum layer could be partially detached from the metal sheet by melting a Surlyn film on top of it and pulling it off) might give rise to additional contact resistance between the Pt layer and metal substrate and thus contribute to the overall ohmic losses as well.

Since plain, uncoated carbon steel is not a suitable building material in reality, based on the results in Publication II stainless steel was chosen as the metal substrate for closer studies.

5.3 Further studies on the suitability of metal materials for DSC substrates (Publications V and VII)

Even if promising efficiencies were measured with the stainless steel CE DSCs, the problem with this cell design is that in order to keep the cell structure completely flexible, the photoelectrode has to be deposited on plastic. Whilst it is possible to prepare satisfactory quality cells with plastic PEs, the mechanical stability and electron transport properties of a compressed-only TiO_2 film are not as good as those of a high-temperature sintered electrode, which is why a reverse design, where the PE is prepared on the steel sheet and the CE on plastic (as a reference also on glass), was developed. Steel substrate tolerates high temperatures, which enables sintering of the PE films and due to its superior electrical conductivity, it is also a promising substrate material for cell size upscaling. Flexible CEs with high catalytic activity and good mechanical and chemical stability, on the other hand, are relatively easy to prepare for example with sputtering platinum on ITO-PET. Figure 27 presents schematics of the stainless steel based DSC geometries.

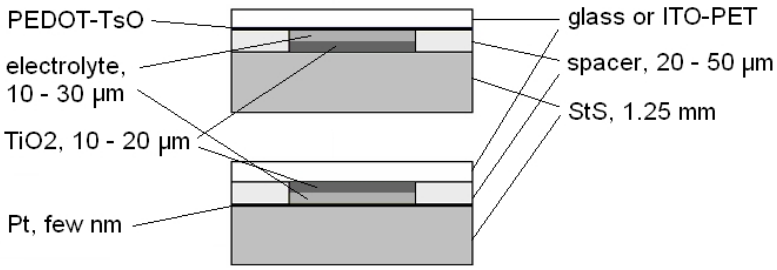

Figure 27. StS-based DSC designs. StS as the PE (upper, here with a PEDOT CE) and as the CE (lower) [78].

The obvious problem in the reverse cell design where light has to enter the photoactive material through CE and electrolyte layers due to the opaqueness of the steel substrate is light absorption in these layers. This shadowing effect can be minimized, though, with optimization of the cell structure.

The optimization of the CE calls for an effective trade-off between the electrode's transmittance and high enough catalytic activity on it. Conducting polymer PEDOT and sputtered Pt were tried as the CE catalysts since deposition of high transparency thin films is possible with both of these materials. Due to uncertainties considering the stability of the PEDOT layers and poorer *IV*-curves measured with PEDOT CE cells [79] 1-4 nm of sputtered Pt was found to be the best option for a high quality, flexible CE on plastic.

Since the species mostly responsible for optical losses in the electrolyte is the strongly colored triiodide ion, minimizing its concentration and the electrolyte layer thickness utilizing the definition for the diffusion limited current density presented in Chapter 2.4.3 turned out to be the best way to reduce the electrolyte's shadowing effect. Other methods such as "bleaching" of the electrolyte, i.e. converting the I_3^- ions to colorless IO^- ions by base treatment, and diluting the whole electrolyte were also studied but the results were not satisfactory. For example, in the dilution of the whole electrolyte also the concentrations of the beneficial electrolyte species such as 4-*tert*-butylpyridine decrease which led to poorer cell efficiencies compared to the cells where only the I_3^- concentration and electrolyte layer thickness were reduced. In short, 16 % gain in the cell efficiency was obtained when decreasing the electrolyte layer thickness from 40 µm to 20 µm and correspondingly, the triiodide concentration from 0.05 M to 0.03 M [78, 79]. Table I summarizes the operating parameters of various DSC types prepared at the time of Publication VII (the 3.8 % obtained with an all-flexible, uncoated StS PE cell was of the world record order for a DSC prepared with the same materials and methods [26]). The semi-solid, gelatinized electrolyte used in some of the cells was introduced in order to improve the mechanical stability of the cells. Gelatinization was achieved with adding 5 wt% of the polymer PVDF-HFP into the standard liquid iodine electrolyte as presented in the literature [30].

Cell type	I_{sc} (mA/cm^2)	V_{oc} (V)	*FF* (%)	η (%)
1	14.0	0.704	0.58	5.8
2	13.6	0.663	0.40	3.6
3	12.2	0.675	0.57	4.7
4	12.4	0.618	0.57	4.3
5	11.8	0.597	0.54	3.8
6	5.9	0.603	0.59	2.1

Table I. *IV*-parameters of several StS-based DSCs vs. the standard cell configuration. Cell types are the following: 1: glass PE, liquid electrolyte, Pt-glass CE (standard DSC); 2: glass PE, liquid electrolyte, StS-CE; 3: StS-PE, liquid electrolyte, Pt-glass CE; 4: StS-PE, gel electrolyte, Pt-glass CE; 5: StS-PE, gel electrolyte, Pt-sputtered ITO-PET CE; 6: StS-PE, gel electrolyte, PEDOT ITO-PET CE [78].

In Publication V, the performance and initial stability of the stainless steel DSCs was investigated further. The most important result was that the substrate-mediated

recombination was almost one order of magnitude smaller from bare StS substrate than from TCO glass and of the same order from dye-covered StS in comparison to dye-covered glass (this mimics the situation in real cells where, during the dye-sensitization process, the dye adsorbs also on the bare substrate on the bottom of the TiO_2 layer pores and is known to suppress recombination [80]) which challenges the assumption presented in the literature, that additional protective layers on top of the StS are needed to block recombination [77]. It was also noticed that there are differences between the recombination properties of glass substrates: The recombination current values reported in Publication V were one or two decades lower than those reported elsewhere in the literature for similarly treated TCO glasses [81, 82]. An effect of the StS substrate on the electrochemical function of the TiO_2 layer was also noticed: Open circuit voltage decay measurements with which it is possible to determine the effective lifetime of electrons in the TiO_2 film showed that more recombination from the TiO_2 occurred in the case of StS substrates compared to glass substrates. This effect was investigated further in other studies but since the author had no contribution to those studies, the results are out of the scope of this thesis. In general, since the author's contribution to Publication V was only marginal, its results were discussed here just briefly.

5.4 Upscaling the metal-based DSC (Publication VI)

Publication VI concentrates on the upscaling issues of the optimized StS-based DSC structure. Even if the cell efficiencies were satisfactory with small, laboratory-size test cells (current generating active areas typically less than 0.5 cm^2) the situation changes when the substrate area increases. The technical challenges in the cell manufacturing are also different with large area cells and at some point the limit when the cells can not be prepared manually in the laboratory anymore but the production line needs to be based on automated equipment is reached. The suitability of the chosen cell concept for large volume, industrial-type manufacturing can, however, be tested with smaller cells, like the 6 cm x 6 cm "mini-modules" prepared for Publication VI.

In our "mini-modules", the reverse cell design where the photoelectrode is deposited on stainless steel sheet and sputter-platinized ITO-PET or ITO-PEN (as a reference, also on TCO glass) worked as the counter electrode was employed. Due to stainless steel's superior conductivity, there is practically no limit to the PE size but on the CE side, the substrate's lateral resistance limits the width of the current collecting area in practice to less than one centimeter. This is why additional current collecting structures are needed on the CE side. In our approach, silver stripes ca. 1 mm of width were applied on the CE substrate, first by hand-painting with conductive silver epoxies and later with inkjet printing with silver nanoparticle ink. The problem of the electrolyte corroding the silver was solved with melting a 3 mm wide Surlyn slices on top of the current collector stripes. The target resistivity of the stripes based on calculations, less than 60 Ω/m, was achieved already with one inkjet-printed layer but to improve the conductivity even further two layers were applied, resulting to resistivity of 23-30 Ω/m with stripe height 2.5-7 µm. This height is still low enough not to short-circuit the cell, considering the thickness of the spacer and sealant Surlyn was 45 µm. In the case of flexible plastic substrates, when

the free area between the Surlyn seals widens to near one cm, the capillary forces tend to bend the plastic in the middle, thus risking the substrates touching each other which is why thicker spacer films are needed for larger area cells. Optical losses in a reverse lighting, thicker spacer cells are also compensated some since the front (plastic) substrate's bending diminishes the distance between the electrodes.

To optimize the large cell structure, i.e. the positioning and geometry of the CE current collector stripes and correspondingly, the width of the TiO_2 stripes on the PE side, a semi-empirical mathematical model was developed [83]. The model was based on partial differential equations describing the current flow in the cell, special emphasis being put on the counter electrode – electrolyte interface. The model was constructed and solved with COMSOL Multiphysics© software and its input consisted of a measured *IV*-curve of a small, laboratory-size test cell and the data about the spatial distribution of the substrate surface conductivities, depending on the substrate material and the location of the current collector structures. The current generation on the PE side was modeled with an "extended" dye solar cell equivalent circuit (Figure 28), as a parallel combination of a photocurrent source term (I_{ph}) and a diode (I_d) describing the recombination current. In another words, the large cell was treated as an "infinite" number of infinitesimally small cells in parallel. With the model, the voltage losses in different parts of the large cell could be calculated (Figure 29) and the structure optimized to minimize those, along with the active area losses bound to occur because of the current collector positioning and protection. Figure 30 presents schematics of the two final large cell configurations, one for cells with TCO glass CE (reference) and another for cells with ITO-PET CE, and Figure 31 photographs of the real cells. In the ITO-PET CE cells, the silver stripes are widened slightly near the main current collector to reduce the ohmic losses due to substrate's sheet resistance as much as possible.

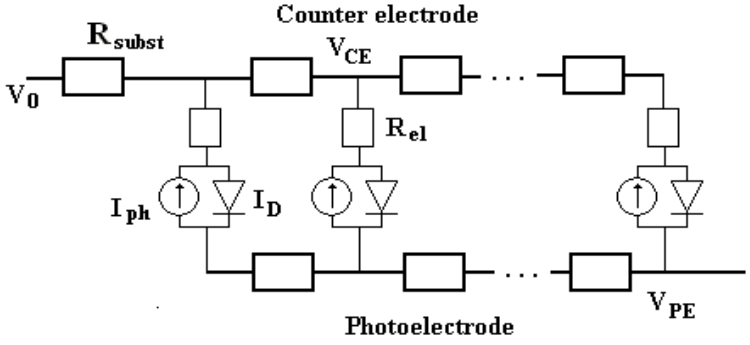

Figure 28. An "extended" DSC equivalent circuit used to model the current generation and voltage losses in a large cell [83].

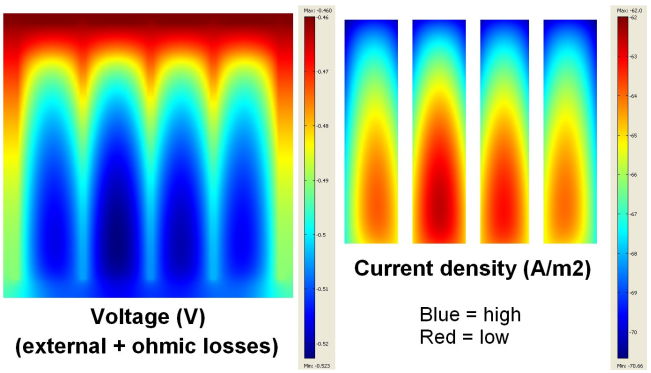

Figure 29. Current densities and voltage losses in a 6 cm x 6 cm DSC "mini-module". In the picture, the main current collector is located on top of the picture which is why the current flow is the most efficient there [83].

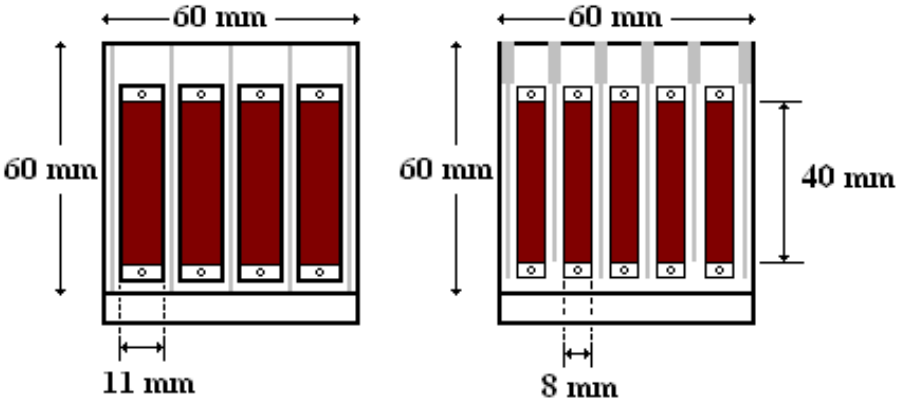

Figure 30. The final geometries for the large cell. On the left for the glass CE cells, on the right for the ITO-PET CE cells. Dark red: dyed TiO_2; light grey: silver stripes. Active areas on both cell types ca. 15 cm^2 [83].

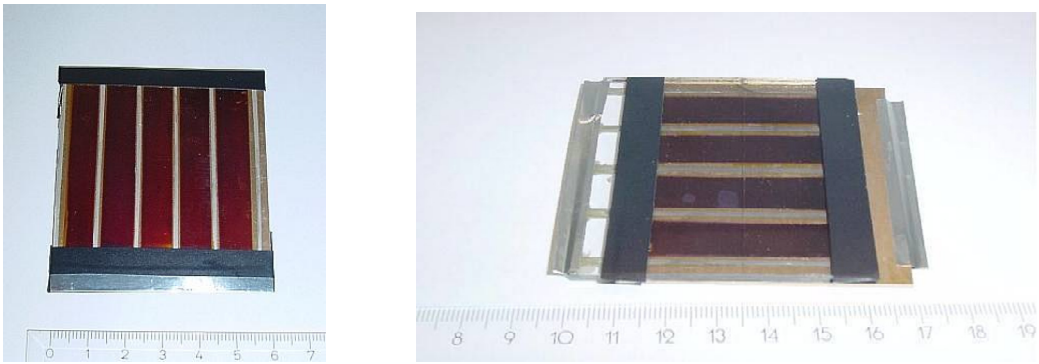

Figure 31. Photographs of StS-based DSC "mini-modules", substrate size 6 cm x 6 cm.

Promising efficiencies were obtained both with glass CE and ITO-PET CE large cells: 3.4 % with a StS PE and thermally platinized glass CE and 2.5 % with a StS PE and sputter-platinized ITO-PET CE (1-4 nm of Pt). Whilst these efficiencies are still relatively low they are, however, of the same order than what have been measured with small cells prepared with the same materials and manufacturing methods. They are also well comparable to literature [23] though again, the StS-based DSC module prepared in [23] was prepared on ITO- and SiO_x-coated steel so the results are comparable only order-wise. This shows that replacing the other substrate with highly conductive steel and embedding the additional current collector structures to another, less conductive substrate is a method worth adopting for even larger DSC module manufacturing. For example, approximately 50 % reduction in total ohmic losses was achieved with the CE current collector stripes and 80 % by using steel instead of glass as the PE substrate.

One of the reasons for the low efficiencies of the large cells can be seen from Figure 29, i.e. uneven current generation and uneven voltage losses in the cell. Unfortunately, this is something that can not be completely avoided in large DSC modules where the current is generated in long, parallel PE stripes and led to an external circuit through wirings located on the top and bottom short edges of the stripes because the total resistance on the substrate surface and in the current collector structures grows larger the farther from the wirings the electron transfer processes occur. On the other hand, it was also noticed that the lateral ohmic losses on the substrates' surfaces affect the cell efficiency surprisingly little: Simulations with the model with different combinations of PE/CE sheet resistivities showed that a StS PE/glass CE cell (sheet resistivities 0/15 Ω/□) gave more than 90 % efficiency and a StS PE/ITO-PET CE cell (sheet resistivities 0/60 Ω/□) more than 80 % efficiency compared to an "ideal" cell with 0/0 Ω/□ sheet resistivities. Based on these observations it can be concluded that the metal-based cell is a promising route towards industrial-scale manufacturing of the DSC modules but special emphasis must be put on the design of the current collector grid on the other, non-metallic substrate. For example, depositing a dense "network" of highly conductive metallic wires of micrometer scale width on top of the PET sheet under the ITO coating (for example with inkjet-printing methods; the ITO coating could then be applied with ALD) could be a successful technique to prepare high quality CE substrates for large area DSC applications. This would also remove the need for additional protective layers on top of the metal wires. In any case, further studies on cell size enlarging call for automated manufacturing methods since cells larger than the 6 cm x 6 cm "mini-modules" prepared for this Publication are very difficult and time-consuming to prepare manually which leads to uneven sample quality and poor statistics of the results.

5.5 Cylindrical DSC structure on optical fiber (Publication VIII)

The motivation behind the optical fiber integrated DSC presented in Publication VIII was to develop an electricity-producing wire with which for example electronic devices located in remote and confined spaces could be powered. PV optical fiber has been realized before with bulk heterojunction blends and solid-state hole conductors [84, 85] but not with the conventional DSC materials and manufacturing methods.

Cylindrical geometry and the non-conductive surface of the fibers obviously present some manufacturing challenges though the latter was easy to overcome with depositing a conductive oxide coating on the fibers with the ALD method. The same method had to be applied also when depositing the TiO_2 layer on PMMA plastic optical fibers since they can not tolerate temperatures much higher than 80 ^oC so sintering as the TiO_2 film post-treatment could not be used. Since the ALD method yields only compact thin films (several tens of nanometers thick) the ALD-deposited PE could obviously not produce currents comparable to proper nanoporous, high active surface area TiO_2 films. The idea could be demonstrated even with this thin TiO_2 layer, though, and on glass fibers a "normal", sintered PE could be prepared with dip-coating from diluted titania paste. PVDF-HFP gelatinized iodine electrolyte [30] which turns liquid when heated to 130 - 140 ^oC but solidifies when cooled again to room temperature was a feasible option to coat the electrolyte layer on top of the dye-sensitized PE and for the counter electrode, a new, gelatinized carbon material was developed. This material was based on the carbon black/graphite/TiO_2 powder suspension described earlier in chapter 4.1 and Publication I. To make the material suitable for dip-coating it was gelatinized with PVDF-HFP. To enable heating of the mixture to 130 – 140 ^oC needed to liquefy the gel, the normally used ethanol was replaced with 3-methoxypropionitrile (MePRN) as the suspension solvent (the boiling point of MePRN is so high that it doesn't vaporize when the gel is heated up, in contrast to ethanol which boils already under 100 ^oC). This gelatinized carbon powder suspension solidified into hard, sturdy films on top of the fiber which enabled application of the current collector contacts and handling of the fibers without risking the counter electrode layer flaking off. Actually, the carbon gel looks like a promising alternative as a low temperature depositable CE material for planar cells as well since even plastic substrates can take temperatures up to 130 – 140 ^oC. The polymer networks inside the CE film improve the mechanical stability of it, making it more "flexible" and tolerable to cell bending. They also "bind" the individual particles of the powder together more efficiently than compressing only, so even thicker CE films with higher catalytic activity could be prepared. Due to its viscosity, the heated gel is also easy to apply with doctor-blading/screen-printing method. Figure 32 presents a schematic of the optical fiber DSC.

Even though the cell manufacturing was possible even on cylindrical substrate such as the fibers, the photocurrents remained on the nA scale and correspondingly, cell efficiencies extremely low. With plastic fibers this is easy to understand because only a very small amount of dye can adsorb on an ALD-coated TiO_2 film and with glass fibers, obviously further optimization of the PE film depositing process is called for to improve the film structure, morphology and adhesion to the fiber. However, the open circuit voltages measured from the fiber DSCs were of the same order than those typically obtained with planar cells: 0.5 V at its best (cf. 0.65 – 0.70 V for planar cells). This indicates that despite the low efficiencies, this kind of a DSC could work for example as a photoactive sensor, monitoring the light propagation in an optical fiber. For final applications, the DSC should also be encapsulated with a film that prevents both moisture penetration into the structure and drying of the electrolyte solvent. Even if the gelatinized electrolyte is solid in room temperatures, the polymer forms only a loose network around

the other electrolyte species, including the solvent molecules and does not prevent their evaporation as such.

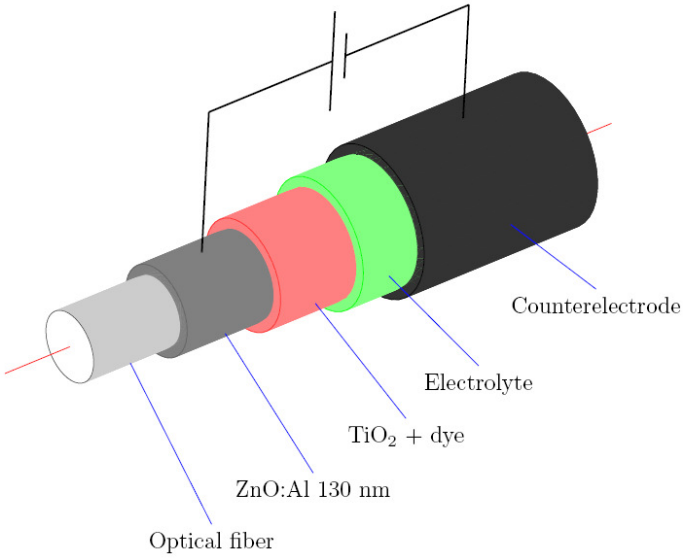

Figure 32. A schematic of a DSC integrated on an optical fiber [86].

5.6 The effect of temperature variations on the fresh and aged DSC performance (Publications III and IV)

The topic of Publications III and IV is a slight sidetrack from the general theme of this thesis, i.e. alternative substrate materials of the DSC to glass but since the effects of temperature variations to the cell performance are an important topic considering the general usability of the cells, these Publications are included in this thesis also.

The initiative behind these studies was an observation, that the performance of an aged, gel electrolyte filled DSC improved when the cell was subjected to heating. A more systematic study was planned, where a large number of cells was stored a certain period of time and their *IV*-curves and EIS spectra were measured as a function of temperature at regular time intervals during this storage period. The cells included in this study were the standard glass cells with photoelectrodes prepared with commercial titania paste or self-made TiO_2 nanoparticle suspension and filled either with liquid or gelatinized iodine electrolyte. In Publication III, the cells were stored in dark and at room temperature for ca. one month and their performance was characterized with *IV*-curve measurements varying the measurement temperature in regular 20 ^{o}C → 40 ^{o}C → 70 ^{o}C → 40 ^{o}C → 20 ^{o}C back and forth ramps. EIS spectra were measured only before and after every temperature ramping. Measurements were made with fresh, two weeks aged and one month aged cells. In Publication IV, the cell types, storage conditions and temperature rampings were similar but now the *IV*-curves were measured only before and after the

temperature treatments whereas the EIS spectra were recorded at every ramp temperature with fresh, ca. two weeks, ca. one month and two and half months aged cells. Also, to uncouple the effect of temperature on the open circuit voltage another set of impedance measurements was performed, where the cell voltage was fixed to 0.6 V, 0.65 V, 0.7 V and 0.75 V with external polarization and the EIS spectra recorded in all those voltages varying the temperature in every voltage in similar ramps as described before. These measurements were performed on one day only.

The most important finding in Publication III was that the overall drop in the efficiency was smaller for temperature-ramped cells than for reference cells that were stored in similar conditions and for the same time and measured at the same days than the temperature-ramped cells but only at room temperature. When averaged over the four different cell types prepared for this study, the efficiency drop was 18 %-unit less for the temperature-treated cells. The most prominent reason for the efficiency degradation over time was decrease in short circuit current whereas the open circuit voltage remained almost the same over the whole observation period. The best cell performance was obtained at 40 ^{o}C though when the temperature was increased to 70 ^{o}C, a radical drop both in I_{sc} and V_{oc} happened. This drop was reversible, though, and when the temperature was lowered in the downward sweep of the ramp, the currents set on higher level than what they had been on in the upward sweep. Actually, the currents remained on this higher level still on the next consecutive measurement day. Figure 33 presents examples of the *IV*-curves before and after the temperature treatments for ca. two weeks aged cells.

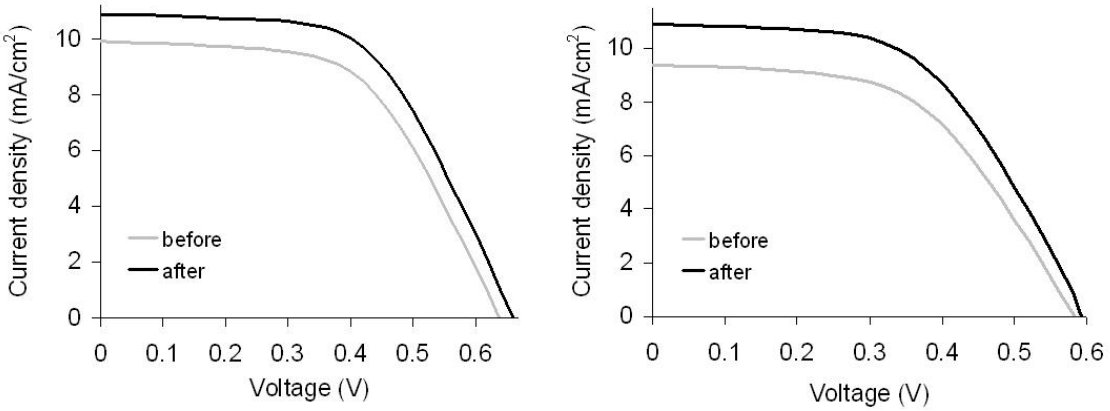

Figure 33. *IV*-curves of ca. two weeks aged cell, before and after the temperature ramping treatment. Left: liquid electrolyte filled cell; right: gel electrolyte filled cell [87].

From the EIS data it could be detected that the electron lifetimes τ_{el} in the TiO_2 film were longer and the charge transfer resistance on the counter electrode lower after the temperature rampings. This can be seen also from Figure 34, where the CE impedance arc in the Nyquist plot is clearly smaller after the temperature treatment and the characteristic frequency of the PE impedance response (i.e. the frequency of the

imaginary impedance peak's maximum) in the Bode plot moves to smaller frequencies f according to equation [16]

$$\tau_e \approx \frac{1}{2\pi f}. \tag{18}$$

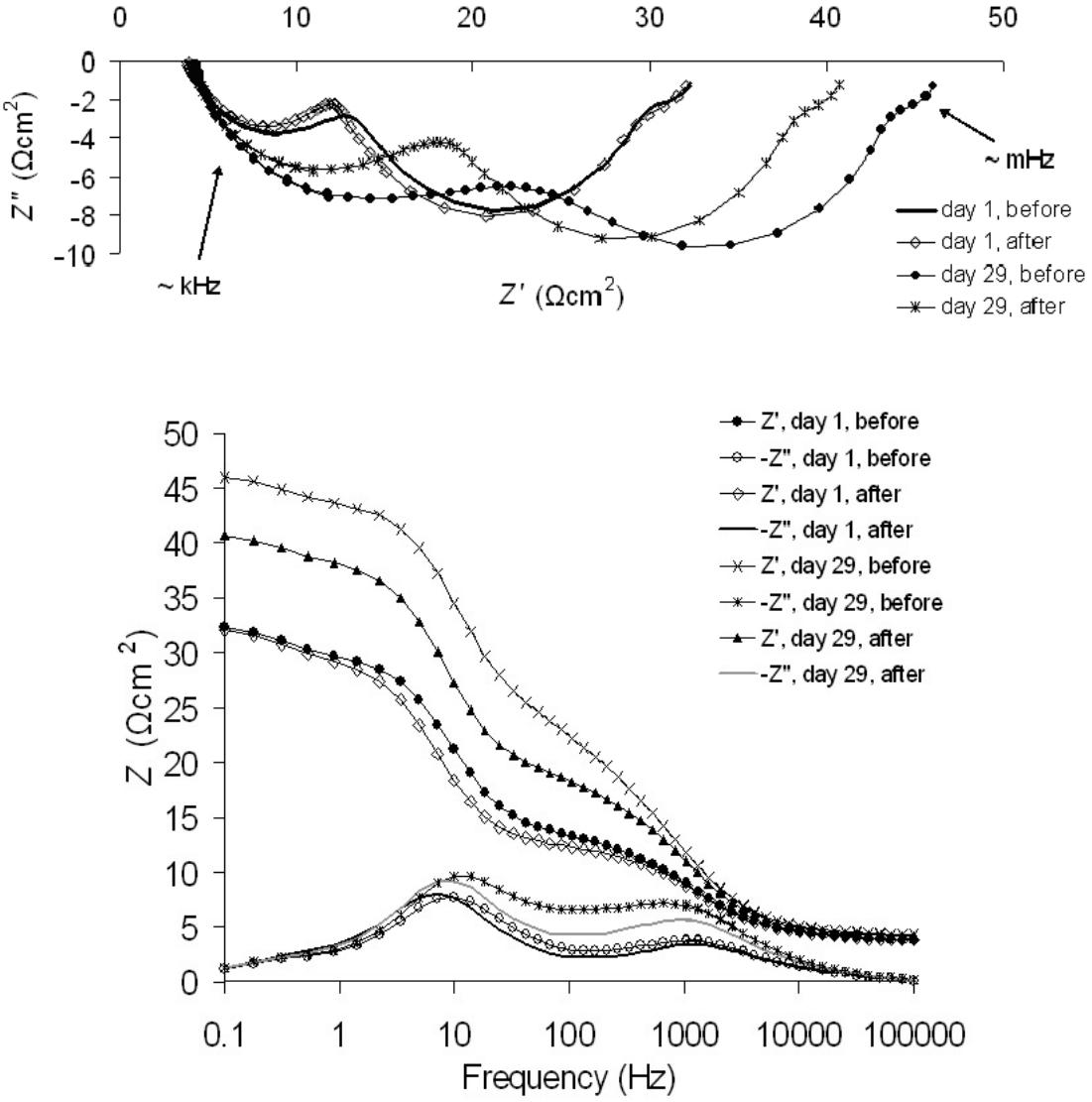

Figure 34. Impedance responses of fresh and ca. one month aged (gel electrolyte filled) cells, before and after the temperature ramping treatment. Top: Nyquist plots; bottom: Bode plots. In the Nyquist plots, the semicircle on the left originates from the CE and the one on the right from the PE. Diffusion impedance arc is halfly overlapped by the PE arc. In the Bode plots, the imaginary impedance peak and the sharp rise in the real impedance on the left originate from the PE and the corresponding characteristics on the right from the CE [87].

The effect of temperature on the CE function also showed some permanence, the charge transfer resistances staying on this lower level even a few hours after the temperature rampings were made. The improvement in the CE catalyst function in elevated temperatures is easy to understand because most catalytes work more efficiently in higher temperatures but the electron lifetime lengthening was a somewhat surprising result. This indicates that the temperature rampings had a positive effect on the recombination suppressing properties of the TiO_2-electrolyte interface – even though as a function of time only, the recombination was noticed to increase. The CE charge transfer resistance increased also as a function of time, indicating deterioration in the CE catalyst. However, the regenerating effect the temperature rampings had on the overall cell performance indicates that instead of being detrimental to the cell operation and long term stability, regularly varying temperature might instead improve those, taken that the temperature does not exceed ca. 60 ^{o}C for extended periods of time. The CE regeneration in the temperature rampings also agrees with [89], where two days of thermal aging improved the CE performance.

The results of Publication IV reflected the results obtained in Publication III. i.e. the aging- and temperature-induced changes in the overall cell performance and the counter electrode function were similar. Due to more detailed EIS measurements, however, more data especially about the behavior of the PE resistance and capacitance could be obtained. For example, it could be detected that the electron transport resistance in the PE film increased over time which indicates deterioration in the PE quality, most likely in interparticle contacts, and that this effect was accentuated at elevated temperatures. This can be seen even visually from Figure 35, where the PE impedance arc of an aged cell undergoes a gradual change from a "clean" semicircle to the Gerischer-shape when the temperature is increased from 20 ^{o}C to 70 ^{o}C. Also, the transport resistance "line" between the PE and CE arcs can clearly be seen in the aged cell's spectrum measured at 40 ^{o}C. In these measurements it must be noted, however, that because the cell voltage was not externally controlled, the V_{oc} was free to vary according to temperature. As the V_{oc} decreases when the temperature increases the increase in R_{tr} (and also in R_{rec}) reflects this. When the V_{oc} is low there are less electrons in the TiO_2 film which hinders efficient charge transport, thus resulting in higher R_{tr}.

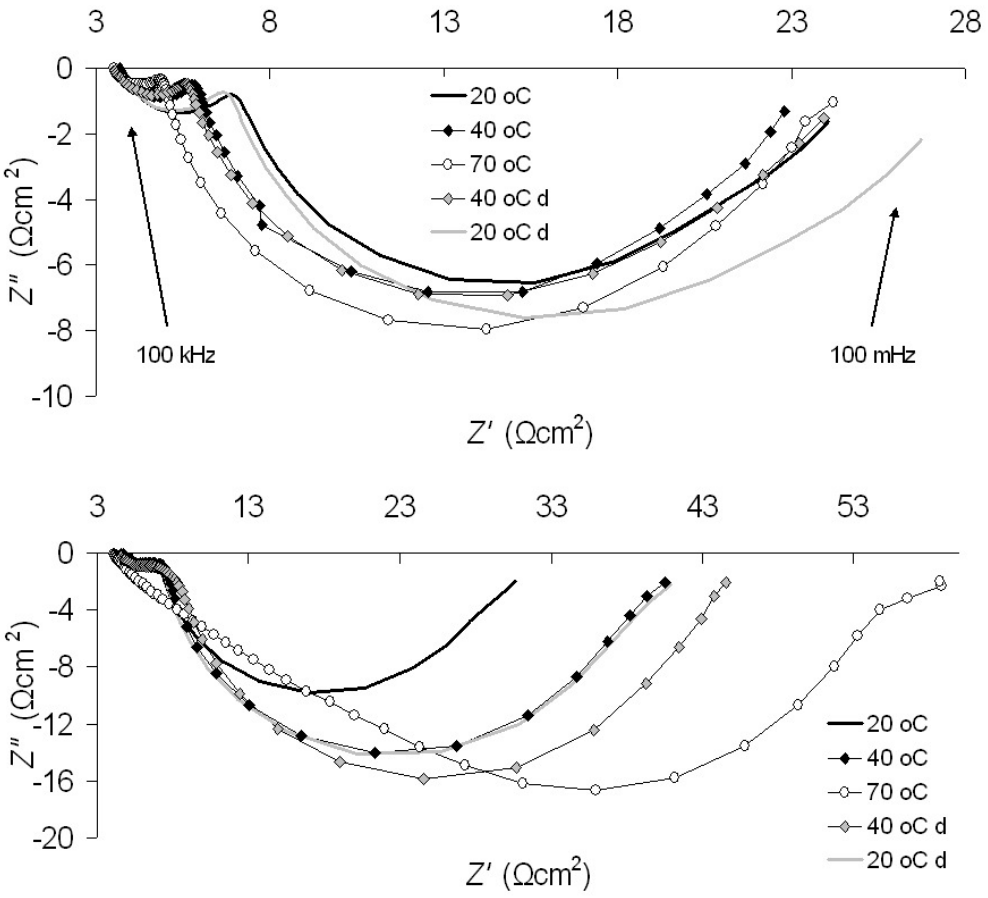

Figure 35. Examples of EIS spectra measured at different temperatures on day one (top) and day 78 (bottom). The letter "d" indicates the downward sweep of the temperature ramp. In the aged cell's spectra the transport resistance "line" shows clearly at 40 °C and the typical Gerischer shape at 70 °C [88].

From those EIS measurements where the cell voltage was fixed with external polarization (so that the effect of the V_{oc} changes with temperature could be eliminated) and the temperature varied it could be seen that both the photoelectrode recombination resistance and the electron transport resistance decreased with temperature. During the downward sweep of the temperature ramp, however, they set on higher than original levels. Higher R_{rec} indicates smaller recombination rate whereas higher R_{tr} detrimental effect of increasing temperature on the electron transport properties of the film. This is consistent with other findings such as the fact that in the earlier measurements, the R_{tr} contributed more to the photoelectrode overall resistance in elevated temperatures especially with the aged cells and that there was regeneration in the short circuit current after the temperature rampings. This latter effect could be at least partially explained with longer electron diffusion length L_e in the film, which is defined as

$$L_e = \sqrt{\frac{R_{rec}}{R_{tr}}} \cdot d \,, \tag{19}$$

where d is the film thickness. Longer diffusion length improves the probability that the electrons reach the current collector before recombination, thus increasing the I_{sc}. However, in general the temperature-induced variation in L_e was quite small and irregular in this study so probably other factors than only that were responsible for the I_{sc} regeneration. L_e's temperature behavior was also contradictory to what had been published previously in [68] though it must be noted here that the measurements in [68] were made in the dark whereas our measurements were performed with lighted cells. The temperature behavior of PE capacitance contradicted results in [68] also – in [68] the C_{pe} was independent of temperature whereas in our experiments, clear (and reversible) increase as a function of temperature was observed. This is in agreement with other publications though, namely [14], where the cells were also measured when lighted. Because the lighting conditions only affect the direction from which the electrons are injected to the PE film (in dark they come from the external circuit and in light, from the dye) where their total amount then sets the V_{oc} which directly affects the capacitance the fact that the capacitance shows temperature dependence only when the electrons come from the dye indicates temperature-dependent changes in the dye-TiO_2 interface or the structure/properties of the dye itself. C_{pe}'s temperature behavior at fixed voltages, when plotted against $1/T$, also indicates temperature-induces shifts in the TiO_2 conduction band energy level and/or redox Fermi level which would also agree with [14].

6 Summary and conclusions

In order to utilize solar electricity's full potential as a clean, renewable energy source new PV device concepts have to be developed alongside the already established, traditional silicon and thin film panels. This thesis concentrates on dye solar cells, a still relatively new type of photovoltaic converter, which promises lie in for the most part cheap, non-toxic and well abundant materials and simple manufacturing methods. However, since the common approach has been to prepare dye solar cells on glass alternative substrate materials need to be found. Whilst glass DSC still gives the highest efficiencies and best results concerning long term stability of the cells, rigid and fragile glass substrate is obviously suitable only for batch process type manufacturing, quite like the silicon and thin film panels as well.

In this thesis alternative substrate materials to glass, namely ITO-PET plastic foils and stainless steel sheets have been investigated. Preparing the cells on flexible, light weight substrates such as plastics enables high throughput roll-to-roll type manufacturing of the cells and widens the variety of applications this cell type could be used in. Plastic-based DSC could power for example portable electronics or could be integrated to textiles or on paper. Stainless steel is not necessarily light weight as such but it is still flexible and also cheap compared to other substrate materials. A very interesting approach would be to coat the DSC on roofing or façade steels to produce electricity-generating building

materials. This would save the additional costs and effort needed in the separate installation of the PV panels and their supporting structures.

Tests with electrode materials and preparation methods suitable for plastic substrates showed that it is possible to prepare for example high quality counter electrodes even without the expensive platinum (the traditionally used CE catalyst) and high temperature post-treatment steps. Widely available, non-toxic and cheap carbon-based materials showed as high catalytic activity than platinum, 0.5 – 2 Ωcm^2 at their best, and the preparation method for the carbon CEs – powder suspension spraying and room temperature compressing – is easily upscaleable to large volume automated manufacturing as well. The drawback of this method is, however, the relatively thick catalyst layers needed which yield opaque electrodes and may risk flaking of the material. This is why long term stability of this kind of CEs is still unsure, especially if the cells are subjected to heavy bending. A solution to this problem could be found, however, from the new carbon-based CE material developed during this thesis, where the carbon powder suspension was made into gel that solidifies in room temperature and yields flexible but still sturdy CE films with efficient adhesion to the CE substrate. All-plastic DSC with spray-coated TiO_2 photoelectrodes and carbon-based counter electrodes is thus a potential alternative to traditional glass-based cells, especially considering the plastic cell efficiencies are already close to 10 % which is not far from the glass cell values anymore and well comparable to for example amorphous silicon cells [48, 49].

Promising efficiencies close to 5 % have been obtained also with stainless steel based cells, and the cell type where the PE was deposited on steel and CE on flexible ITO-PET foil was chosen for cell size upscaling tests as well. Depositing the PE on the steel sheet enables high temperature sintering as the post-treatment, yielding better quality electrodes both efficiency- and stability-wise than compressing only. In the upscaling tests it was also noticed that a significant 80 % decrease in total ohmic losses of the cell was achieved when the PE's glass substrate was replaced with steel, due to steel's superior conductivity. The largest cells prepared in the course of this thesis were 6 cm x 6 cm but drastic enlargening of the cell size is possible using the steel substrates and optimizing the counter electrode and electrolyte structure. CE and electrolyte optimization is needed because, due to steel's opaqueness, the light has to enter the photoactive layer through the CE and electrolyte which obviously leads to optical losses. Also, due to relatively poor lateral conductivity of the ITO-plastic films additional current collectors have to be integrated on the CE substrate. We achieved good results with inkjet-printed silver nanoparticle ink with which thin current collector wires were deposited on the ITO-PET to reduce the distance the electrons had to travel before reaching the main current collectors on the outer edges of the cell. With this approach, approximately 50 % reduction in ohmic losses was obtained. The best efficiencies measured with 6 cm x 6 cm steel cells were around 3 %, which is already on the same level than what has been obtained with small, laboratory-size test cells prepared with the same materials and manufacturing methods. Of course, 3 % is still a low efficiency and room for improvement exists but the possibility to prepare the cells in large volumes still keeping the manufacturing process cheap, production of even relatively low efficiency cells becomes economically feasible.

Even if the route to transfer the DSC technology from the traditional glass substrates to cheap and flexible metals and plastics suitable for cost-efficient, high throughput industrial scale production seems relatively simple, i.e. materials and manufacturing methods for this do exist and even the cell efficiencies are already on promising level, there are still several issues that need closer investigation before these kind of cells can be marketed to regular consumers. For example, during this thesis work stability problems of the steel-based cells have arisen and research on those is under way at the moment. As a matter of fact, on the field of DSC research in general, relatively little is still known about the exact processes that affect the cells' stability and what should be done to improve it. One problem is also that, due to the fact that the DSC is still a rather new concept on the field of PV, no standardized stability characterization tests such as exist for example for silicon panels have been developed. So, in order to utilize the full potential of the DSC technology and make this solar cell type truly attractive and interesting to both industrial quarters and private customers serious and thorough research effort should be put on identifying the mechanisms that still limit the cells' long term stability and ways to properly and reliably overcome those. Obviously, some efficiency-improvement is also called for – even if the laboratory efficiencies are over 10-11 % already for glass cells the situation changes when the substrate changes, cell size increases and the cells are combined to modules. An interesting solution to this might come from the carbon nanotechnology which recent inventions with novel, highly conductive and catalytic nanoscale materials could potentially improve the DSC performance as well.

References

[1] O'Regan, B.; Grätzel, M., Nature 353, 737-740 (1991).
[2] Grätzel, M., Journal of Photochemistry and Photobiology A: Chemistry 164, pp. 3-14 (2004).
[3] Hara, K.; Arakawa H., Handbook of Photovoltaic Science and Engineering, edited by Luque, A. and Hegedus, S., pp. 663-700, John Wiley & Sons, Inc., England, 2003.
[4] Tulloch, G., Journal of Photochemistry and Photobiology A: Chemistry 164, pp. 209-219 (2004).
[5] Grätzel, M., Current Applied Physics 6 (suppl. 1), pp. e2-e7 (2006).
[6] Nazeeruddin, M.; Péchy, P.; Renouard, S.; *et al.*, Journal of the American Chemical Society 123, pp. 1613-1624 (2001).
[7] Nazeeruddin, M.; Bessho, T.; Cevey, L; *et al.*, Journal of Photochemistry and Photobiology A: Chemistry 185, pp. 331-337 (2007).
[8] http://www.epia.org/home.html, accessed 27 October, 2009.
[9] http://en.wikipedia.org/wiki/World_energy_resources_and_consumption, accessed 27 October, 2009.
[10] http://www.solarbuzz.com/, accessed 27 October, 2009.
[11] http://www.shell.com/, accessed 27 October, 2009.
[12] http://www.bp.com, accessed 27 October, 2009.
[13] http://en.wikipedia.org/wiki/Dye-sensitized_solar_cell, accessed 27 October, 2009.
[14] O'Regan, B.; Durrant, J.; Journal of Physical Chemistry B 110, pp. 8544-8547 (2006).
[15] Bisquert, J., Journal of Physical Chemistry B 108, pp. 2323-2332 (2004).
[16] Kern, R.; Sastrawan, R.; Ferber, J.; Stangl, R.; Luther, J., Electrochimica Acta 47, pp. 4213-4225 (2002).
[17] Peter, L.; Duffy, N.; Wang, R.; Wijayantha, K., Journal of Electroanalytical Chemistry 524-525, pp. 127-136 (2002).
[18] Murakami, T.; Grätzel, M., Inorganica Chimica Acta 361, pp. 572-580 (2008).
[19] Miettunen, K.; Halme, J.; Toivola, M.; Lund, P., Journal of Physical Chemistry C 112, pp. 4011-4017 (2008).
[20] Ma, T.; Fang, X.; Akiyama, M.; Inoue, K.; Noma, H.; Abe, E., Journal of Electroanalytical Chemistry 574, pp. 77-83 (2004).
[21] Fang, X.; Ma, T.; Akiyama M.; Guan, G.; Tsunematsu S.; Abe, E., Thin Solid Films 472, pp. 242-245 (2005).
[22] Toivola, M.; Ahlskog, F.; Lund, P., Solar Energy Materials and Solar Cells 90, pp. 2881-2893 (2006).
[23] Jun, Y.; Kim, J.; Kang, M., Solar Energy Materials and Solar Cells 91, pp. 779-784 (2007).
[24] Ito, S.; Ha, N-L.; Rothenberger, G.; Liska, P.; Comte, P.; Zakeeruddin, S.; Péchy, P.; Nazeeruddin, M.; Grätzel, M., Chemical Communications, pp. 4004-4006 (2006).
[25] Onoda, K.; Ngamsinlapasathian, S.; Fujieda, T.; Yoshikawa, S., Solar Energy Materials and Solar Cells 91, pp. 1176-1181 (2007).

[26] Kang, M.; Park, N.; Ryu, K.; Chang, S.; Kim, K., Chemistry Letters 34, pp. 804-805 (2005).
[27] Park, H.; Jun, Y.; Yun, H.; Lee, S.; Kang, M., Journal of the Electrochemical Society 155, pp. F145-F149 (2008).
[28] Ke, L.; Dolmanan, S.; Shen, L.; Pallathadk, P.; Zhang, Z.; Lai, D.; Liu, H., Solar Energy Materials and Solar Cells 94, pp. 323-326 (2010).
[29] Zhang, Z.; Zakeeruddin, S.; O'Regan, B.; Humphry-Baker, R.; Grätzel, M., Journal of Physical Chemistry B 109, pp. 21818-21824 (2005).
[30] Wang, P.; Zakeeruddin, S.; Grätzel, M., Journal of Fluorine Chemistry 125, pp. 1241-1245 (2004).
[31] Tennakone, K.; Kumara, G.; Kottegoda, I.; Wijayantha, K.; Perera, V., Journal of Physics D: Applied Physics 31, pp. 1492-1496 (1998).
[32] Kumara, G.; Konno, A.; Shiratsuchi, K.; Tsukahara, J.; Tennakone, K., Chemistry of Materials 14, pp. 954-955 (2002).
[33] Konno, A.; Kitagawa, T.; Kida, H.; Kumara, G.; Tennakone, K., Current Applied Physics 5, pp. 149-151 (2005).
[34] Kumara, G.; Konno, A.; Senadeera, G.; Jayaweera, P.; De Silva, D.; Tennakone, K., Solar Energy Materials and Solar Cells 69, pp. 195-199 (2001).
[35] O'Regan, B.; Lenzmann, F.; Muis, R.; Wienke, J., Chemistry of Materials 14, pp. 5023-5029 (2002).
[36] Perera, V.; Senevirathna, M.; Pitigala, P.; Tennakone, K., Solar Energy Materials and Solar Cells 86, pp. 443-450 (2005).
[37] Tennakone, K.; Senadeera, G.; De Silva, D.; Kottegoda, I., Applied Physics Letters 77, pp. 2367-2369 (2000).
[38] Krüger, J.; Plass, R.; Cevey, L.; Piccirelli, M.; Grätzel, M., Applied Physics Letters 79, pp. 2085-2087 (2001).
[39] Krüger, J.; Plass, R.; Grätzel, M.; Matthieu, H-J., Applied Physics Letters 81, pp. 367-369 (2002).
[40] Schmidt-Mende, L.; Bach, U.; Humphry-Baker, R.; Horiuchi, T.; Miura, H.; Ito, S.; Uchida, S.; Grätzel, M., Advanced Materials 17, pp. 813-815 (2005).
[41] Saito, Y.; Fukuri, N.; Senadeera, R.; Kitamura, T.; Wada, Y.; Yanagida, S., Electrochemistry Communications 6, pp. 71-74 (2004).
[42] Hauch, A.; Georg, A., Electrochimica Acta 46, pp. 3457-3466 (2001).
[43] Gorlov, M.; Kloo, L., Dalton Transactions, pp. 2655-2666 (2008).
[44] Gorlov, M.; Pettersson, H.; Hagfeldt, A.; Kloo, L., Inorganic Chemistry 46, pp. 3566-3575 (2007).
[45] O'Mahony, A.; Silvester, D.; Aldous, L.; Hardacre, C.; Compton, R., Journal of Chemical and Engineering Data 53, pp. 2884-2891 (2008).
[46] Papageorgiou, N.; Maier, W.; Grätzel, M., Journal of the Electrochemical Society 144, pp. 876-884 (1997).
[47] Sastrawan, R.; Beier, J.; Belledin, U.; *et al.*, Progress in Photovoltaics: Research and Applications 14, pp. 697-709 (2006).
[48] Green, M.; Emery, K.; Hishikawa, Y.; Warta, W., Progress in Photovoltaics: Research and Applications 16, pp. 435-440 (2008).
[49] Yamaguchi, T.; Tobe, N.; Matsumoto, D.; Arakawa, H., Chemical Communications, pp. 4767-4769 (2007).

[50] Zhang, D.; Yoshida, T.; Minoura, H.; Chemistry Letters, pp. 874-875 (2002).
[51] Zhang, D.; Yoshida, T.; Minoura, H.; Advanced Materials 15, pp. 814-817 (2003).
[52] Tan, W.; Chen, J.; Zhou, X.; Zhang, J.; Lin, Y.; Li, X.; *et al.*, Journal of Solid State Electrochemistry 13, pp. 651-656 (2009).
[53] Miyasaka, T.; Kijitori, Y.; Murakami, T.; Kimura, M.; Uegusa, S., Chemistry Letters, pp. 1250-1251 (2002).
[54] Murakami, T.; Kijitori, Y.; Kawashima, N.; Miyasaka, T., Chemistry Letters 32, pp. 1076-1077 (2003).
[55] Lee, J.; Coia, G.; Lewis, N., Journal of Physical Chemistry B 108, pp. 5282-5293 (2004).
[56] Uchida, S.; Tomiha, M.; Takizawa, H.; Kawaraya M., Journal of Photochemistry and Photobiology A: Chemistry 164, pp. 93-96 (2004).
[57] Pan, H.; Ko, S.; Misra, N.; Grigoropoulos, C., Applied Physics Letters 94, pp. 071117/1-3 (2009).
[58] Wang, P.; Zakeeruddin, S.; Moser, J.; Nazeeruddin, M.; Sekiguchi, T.; Grätzel, M., Nature Materials 2, pp. 402-407 (2003).
[59] Grätzel, M., Chemistry Letters 34, pp. 8-13 (2005).
[60] Hinsch, A.; Kroon, J.; Kern, R.; Uhlendorf, I.; Holzbock, J.; Meyer, A.; Ferber, J., Progress in Photovoltaics: Research and Applications 9, pp. 425-438 (2001).
[61] http://www.dyesol.com/, accessed 27 October, 2009.
[62] http://www.g24i.com/, accessed 27 October, 2009.
[63] http://www.konarka.com/, accessed 27 October, 2009.
[64] Emery, K., Handbook of Photovoltaic Science and Engineering, edited by Luque, A. and Hegedus, S., pp. 701-752, Wiley, England, 2003.
[65] Macdonald, J., Impedance Spectroscopy, Wiley, England, 1987.
[66] Bisquert, J.; Garcia-Belmonte, G.; Fabregat-Santiago, F.; Ferriols, N.; Bogdanoff, P.; Pereira, E., Journal of Physical Chemistry B 104, pp. 2287-2298 (2000).
[67] Fabregat-Santiago, F.; Bisquert, J.; Garcia-Belmonte, G.; Boschloo, G.; Hagfeldt, A., Solar Energy Materials and Solar Cells 87, pp. 117-131 (2005).
[68] Wang, Q.; Ito, S.; Grätzel, M.; Fabregat-Santiago, F.; Mora-Seró, I.; Bisquert, J.; Bessho, T.; Imai, H., Journal of Physical Chemistry B 110, pp. 25210-25221 (2006).
[69] Bisquert, J.; Garcia-Belmonte, G., Fabregat-Santiago, F.; Ferriols, N.; Bogdanoff, P.; Pereira, E., Journal of Physical Chemistry B 104, pp. 2287-2298 (2000).
[70] Imoto, K.; Takahashi, K.; Yamaguchi, T.; Komura, T.; Nakamura, J.; Murata, K., Solar Energy Materials and Solar Cells 79, pp. 459-469 (2003).
[71] Lindström, H.; Holmberg, A.; Magnusson, E.; Lindquist, S.; Malmqvist, L.; Hagfeldt, A., Nano Letters 1, pp. 97-100 (2001).
[72] Kitamura, T.; Maitani, M.; Matsuda, M.; Wada, Y.; Yanagida, S., Chemistry Letters, pp. 1054-1055 (2001).
[73] Halme, J.; Toivola, M.; Tolvanen, A.; Lund, P., Solar Energy Materials and Solar Cells 90, pp. 872-886 (2006).
[74] Fang, X.; Ma, T.; Guan, G.; Akiyama, M.; Kida T.; Abe, E., Journal of Electroanalytical Chemistry 570, pp. 257-263 (2004).
[75] Saito, Y.; Kubo, W.; Kitamura, T.; Wada Y.; Yanagida, S., Journal of Photochemistry and Photobiology A: Chemistry 164, pp. 153-157 (2004).
[76] Baxter, J.; Aydil, E., Solar Energy Materials and Solar Cells 90, pp. 607–622 (2006).

[77] Kang, M.; Park, N.; Ryu, K.; Chang, S.; Kim, K., Solar Energy Materials and Solar Cells 90, pp. 574-581 (2006)
[78] Toivola, M.; Miettunen, K.; Halme, J.; Lund, P., NSTI Nanotech - The Nanotechnology Conference and Trade Show, Boston, U.S.A, June 1-5, 2008, Technical Proceedings of the CTSI Clean Technology and Sustainable Industries Conference and Trade Show, pp. 96-99 (2008).
[79] Miettunen, K., Loss mechanisms and optimization of dye-sensitized solar cells deposited on stainless steel substrates, Master's Thesis, Helsinki University of Technology, 2006.
[80] Sastrawan, R.; Renz, J.; Prahl, C.; Beier, J.; Hinsch, A.; Kern, R., Journal of Photochemistry and Photobiology A: Chemistry 178, pp. 33-40 (2006).
[81] Cameron, P.; Peter, L.; Hore, S., Journal of Physical Chemistry B 109, pp. 930-936 (2005).
[82] Cameron, P.; Peter, L., Journal of Physical Chemistry B 107, pp. 14394-14400 (2003).
[83] Peltola, T., Considerations in designing dye-sensitized solar cell modules, Master's Thesis, Helsinki University of Technology, 2009.
[84] Liu, J.; Namboothiry, M.; Carroll, D., Applied Physics Letters 90, 063501 (2007).
[85] Fan, X.; Chu, Z.; Chen, L.; Zhang, C.; Wang, F.; Tang, Y.; Sun, J.; Zou, D., Applied Physics Letters 92, 113510 (2008).
[86] Toivola, M.; Ferenets, M.; Lund, P.; Harlin, A., Thin Solid Films 517, pp. 2799-2802 (2009).
[87] Toivola, M.; Peltokorpi, L.; Halme, J.; Lund, P., Solar Energy Materials and Solar Cells 91, pp. 1733-1742 (2007).
[88] Toivola, M.; Halme, J.; Peltokorpi, L.; Lund, P., International Journal of Photoenergy 2009, Article ID 786429 (2009).
[89] Wang, Q.; Moser, J.; Grätzel, M., Journal of Physical Chemistry B 109, pp. 14945-14953 (2005).

ISBN 978-952-60-3069-2
ISBN 978-952-60-3070-8 (PDF)
ISSN 1795-2239
ISSN 1795-4584 (PDF)